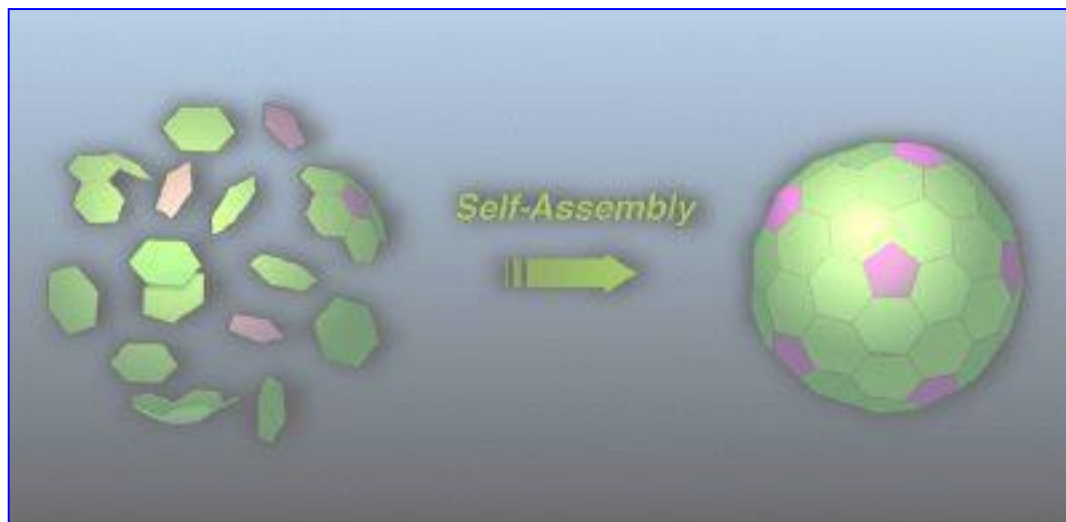
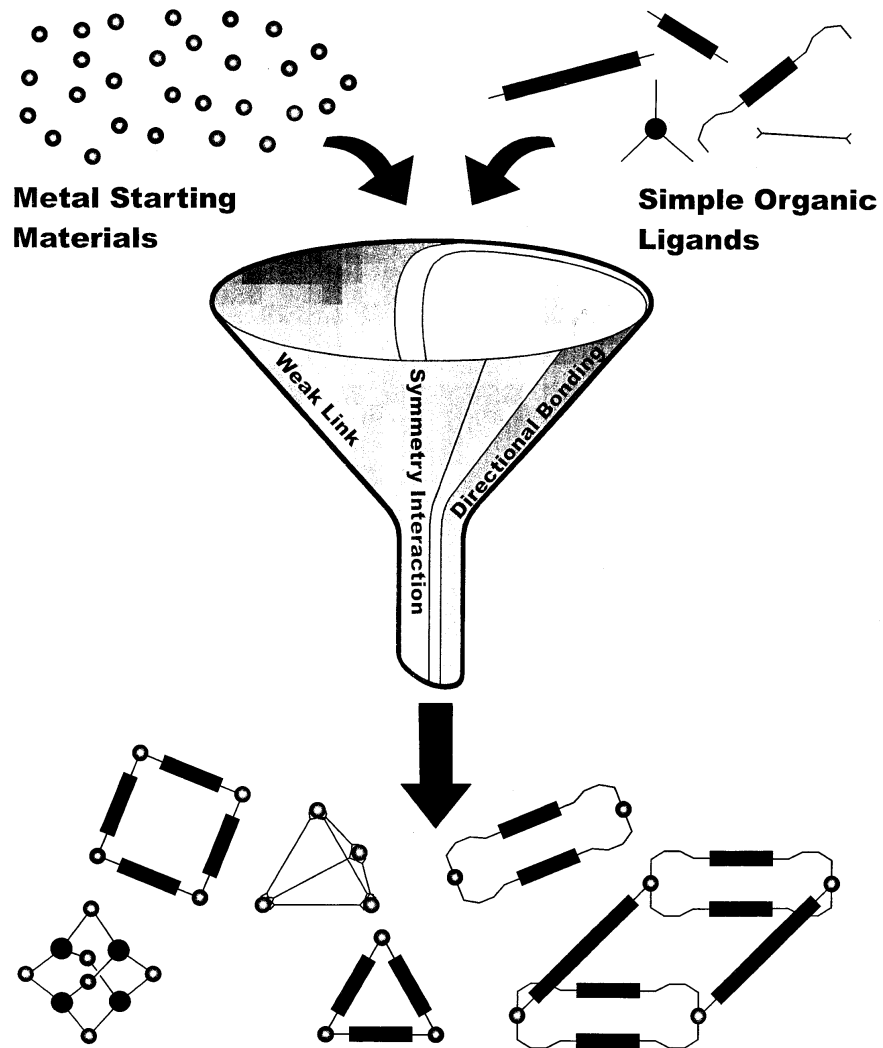


Self-Assembly

The **spontaneous and reversible** association of molecular species to form larger, more complex supramolecular entities according to the **intrinsic information** contained in the components.

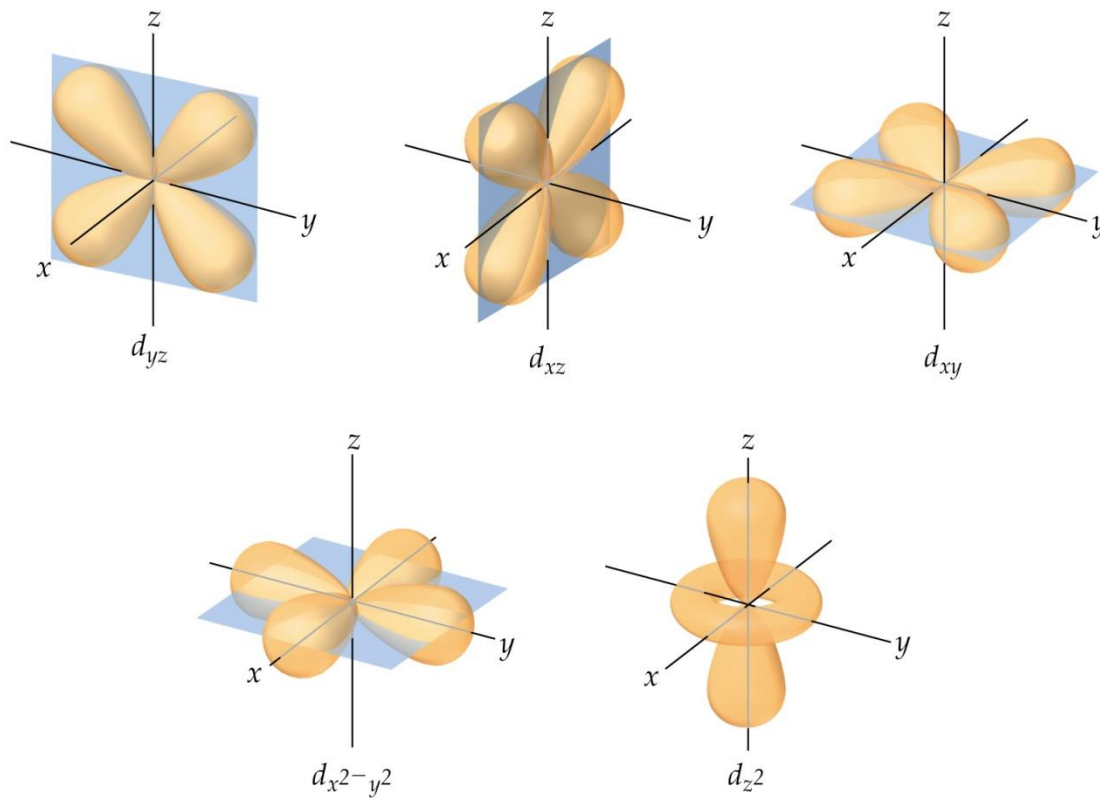


Supramolecular Coordination Chemistry



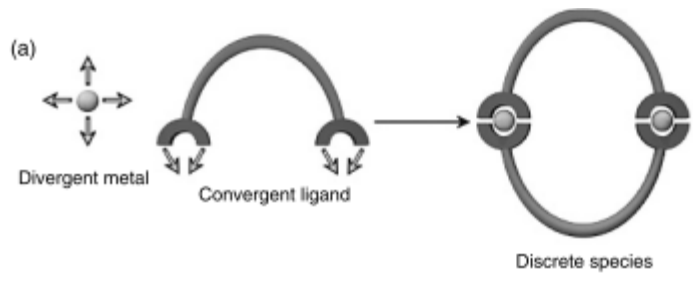
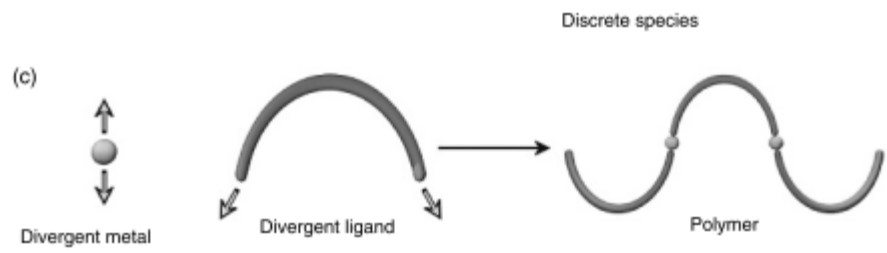
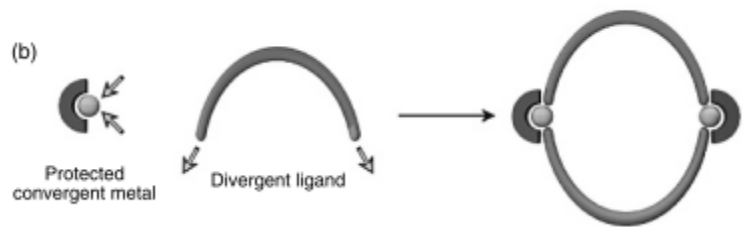
Metal as **connector** :

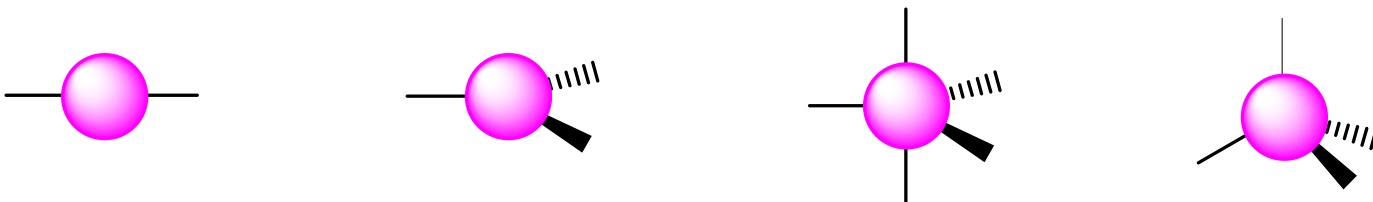
- labile M-L interaction (kinetic)
- stable compound (thermodynamic)
- highly directional with many geometries available



Metal as **functional group** :

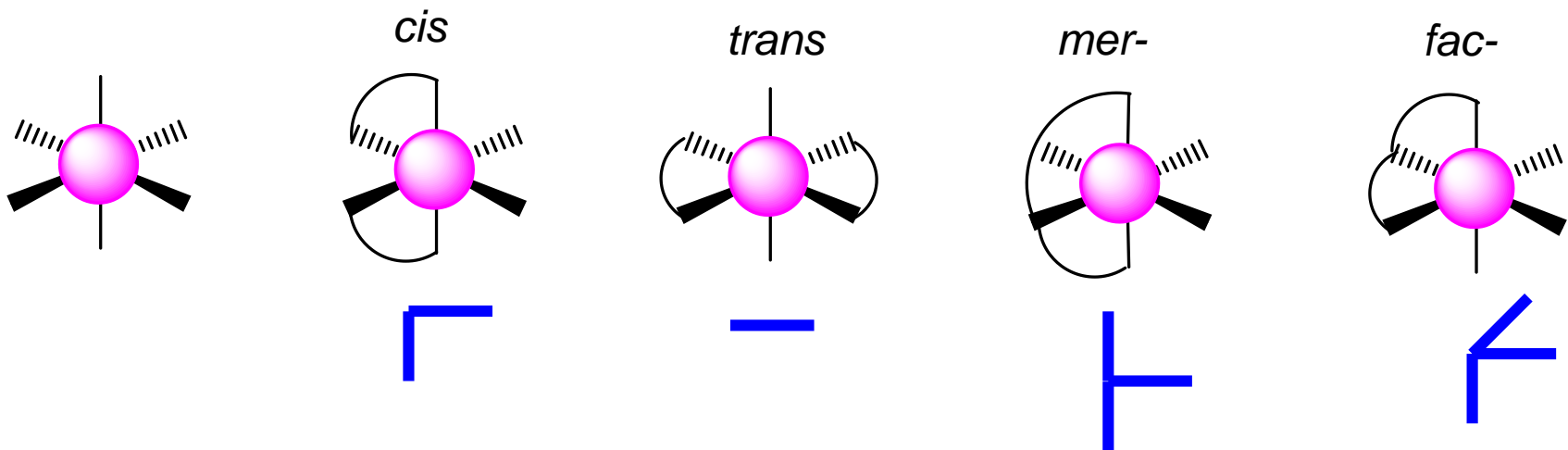
- redox active (electron transfer)
- UV-vis active (color)
- photo active (phosphorescence)
- magnetic properties





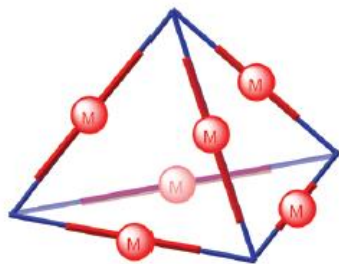
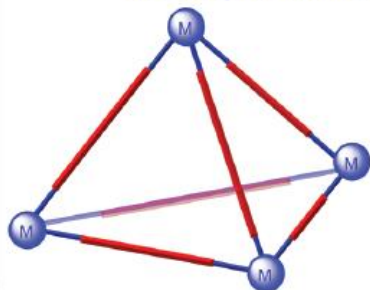
Classical metals used:

Pd(II), Pt(II), Cu(I), Cu(II),
 Re(I), Co(II), Fe(II), Ag(I),
 Zn(II), Ru(II)...

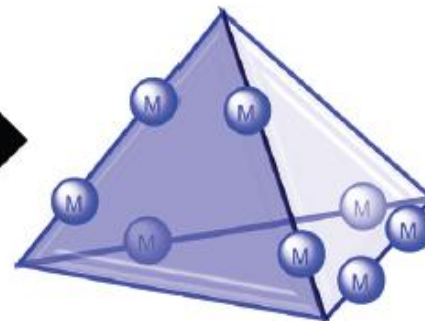
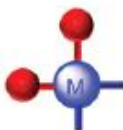


Directional Bonding

60° tritopic subunits + 180° ditopic subunits

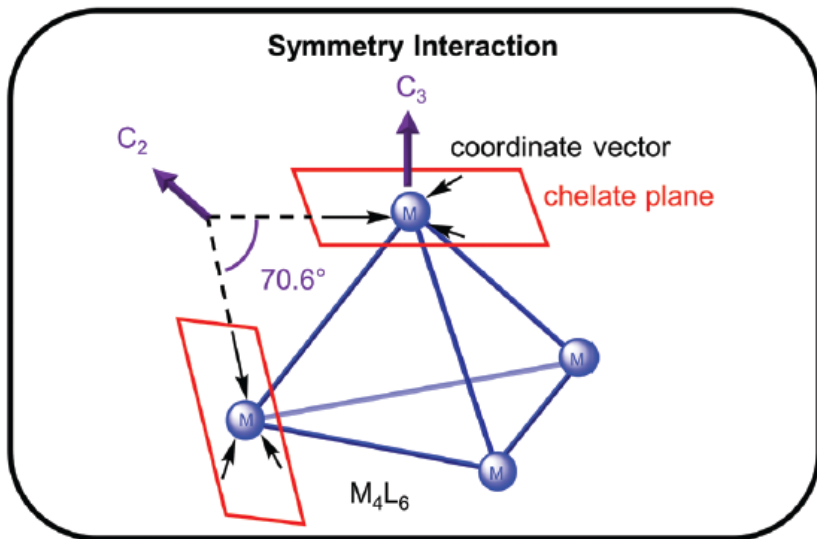


Molecular Panelling

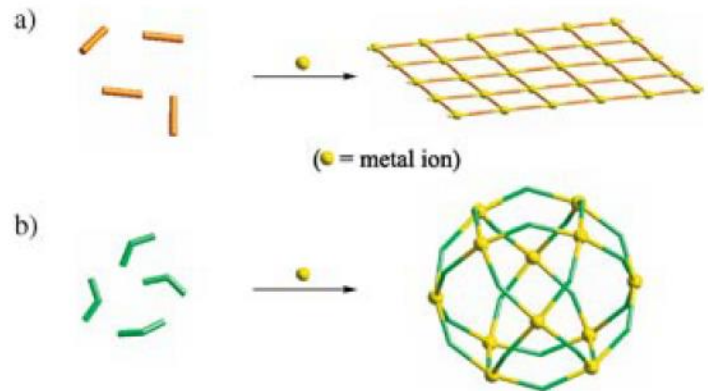


2D panel

M_8L_4

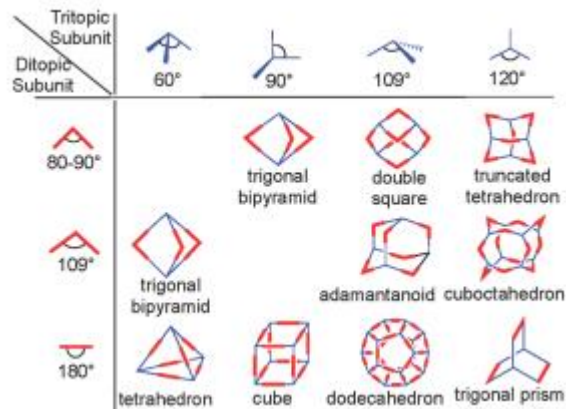
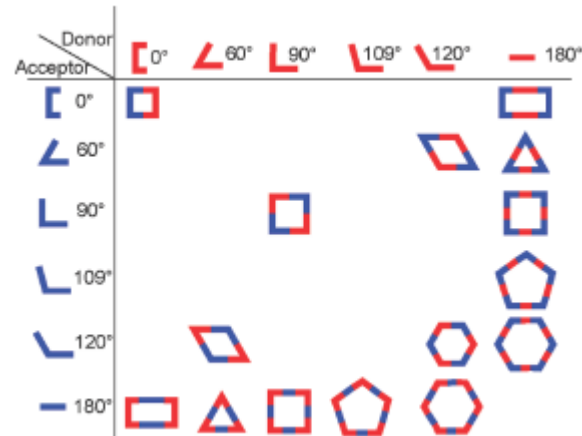


Banana-shaped ligands

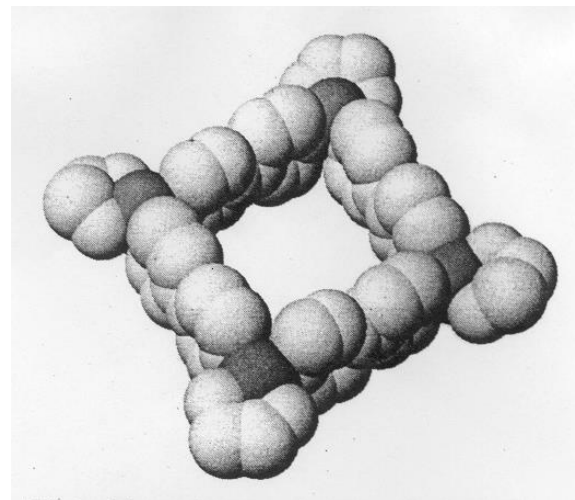
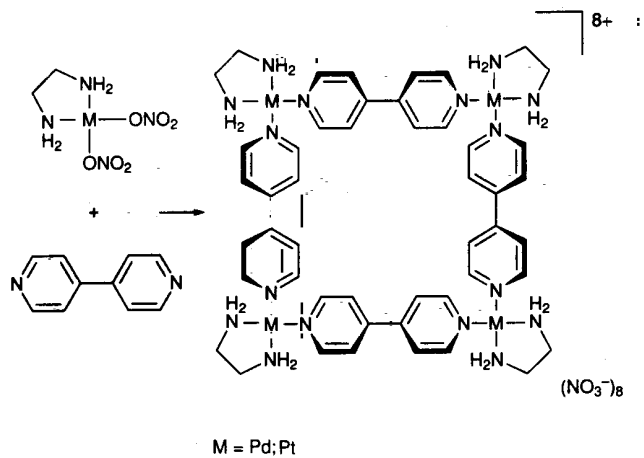


Directonal Bonding Approach

M = bb acido, **L** = bb basico, definiti secondo il numero e geometria relativa dei siti acidi e basici



2D discrete species



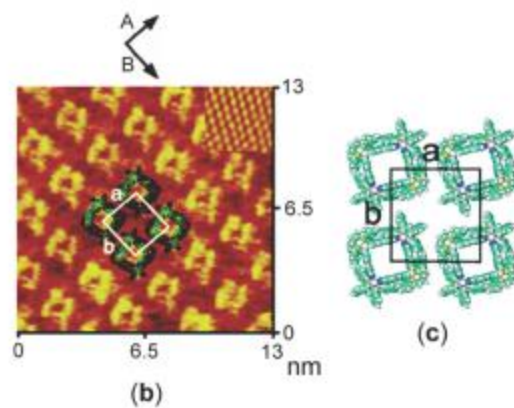
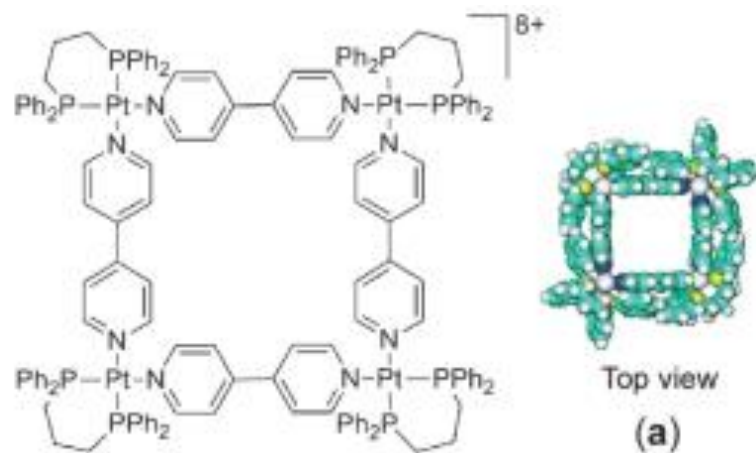
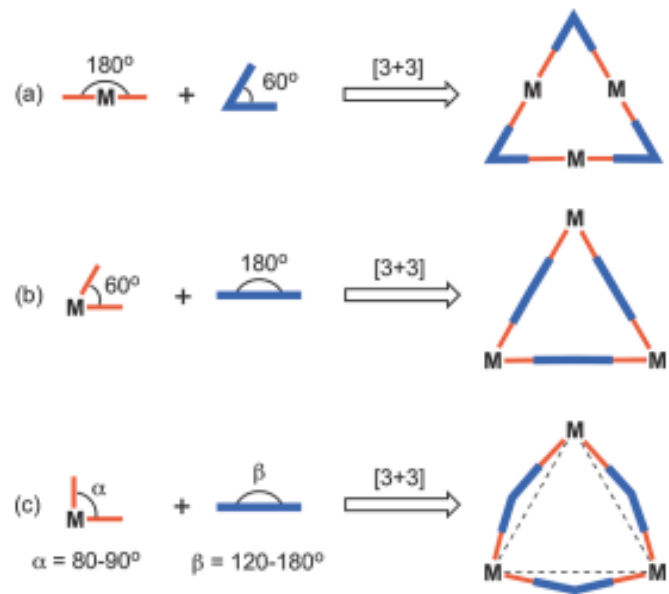
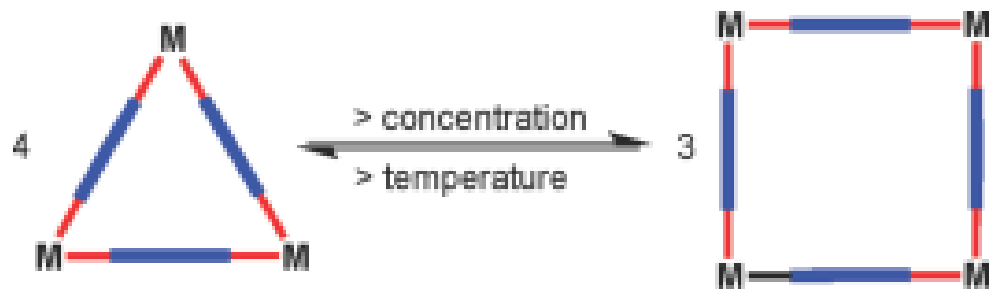


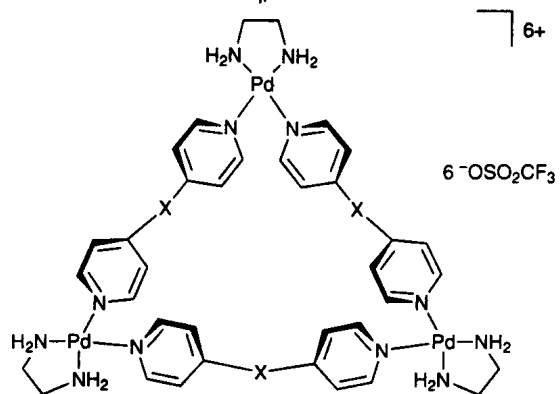
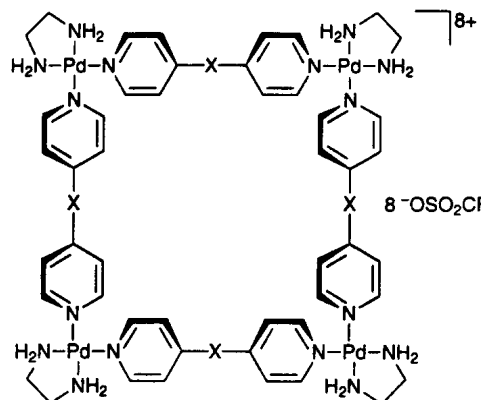
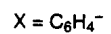
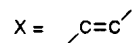
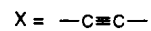
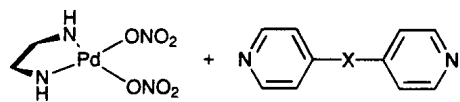
Figure 41. (a) Space-filling model of molecular square $[\text{Pt}(\text{dppp})(4,4'\text{-bipyridine})]_4(\text{PF}_6)_8$, (b) high-resolution STM images of the adlayer of square on Au(111), and (c) structural model of the adlayer.

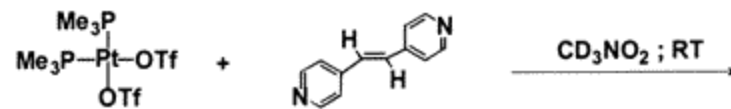
Molecular Triangles





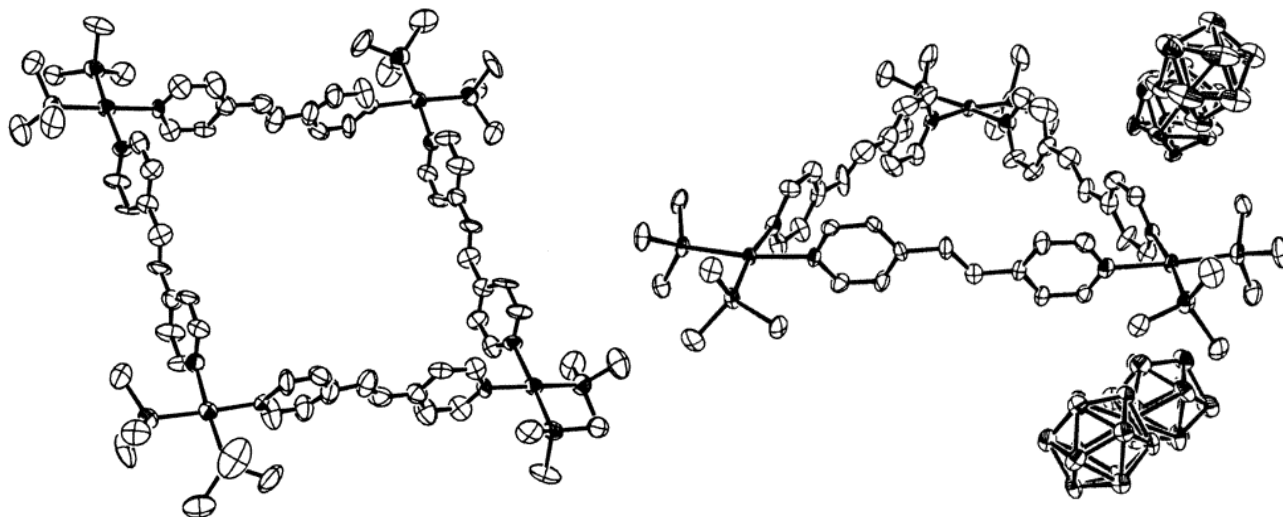
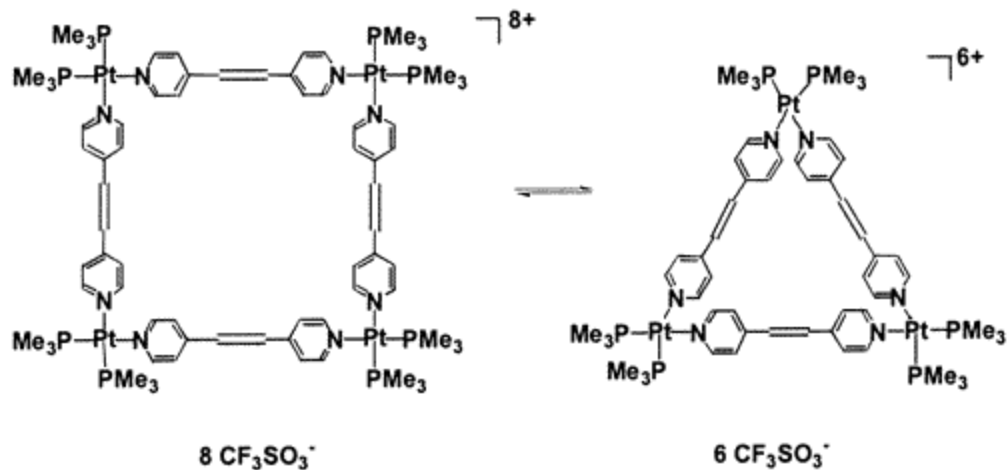
Solvent
Concentration
Temperature

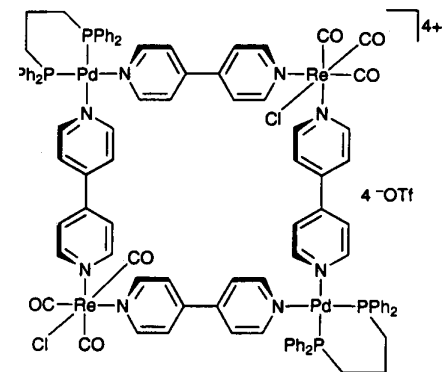
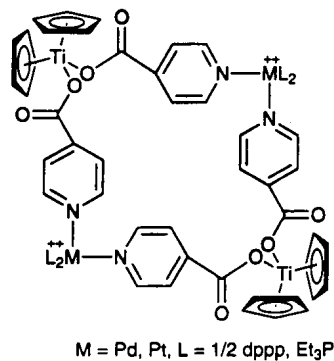
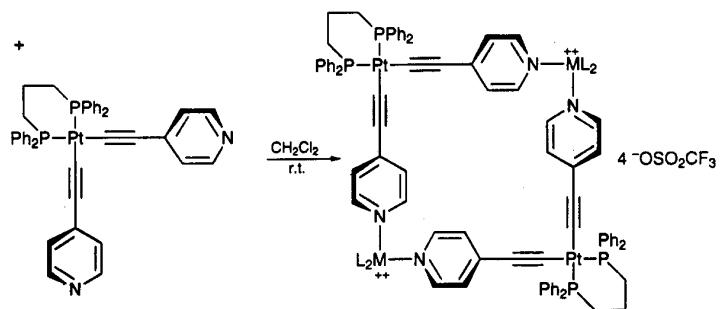
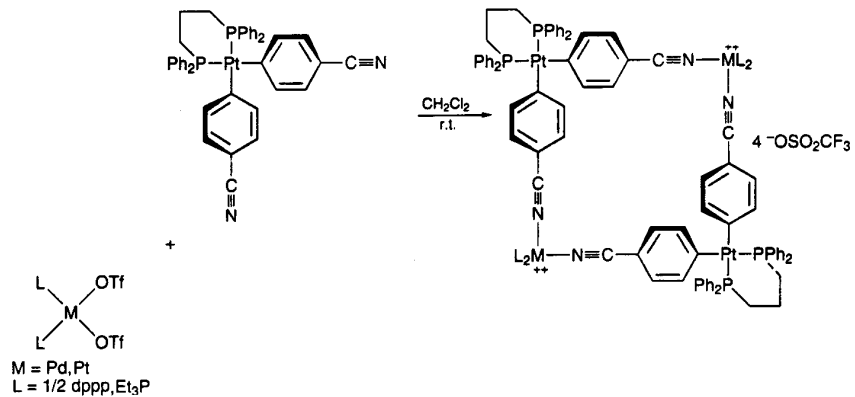


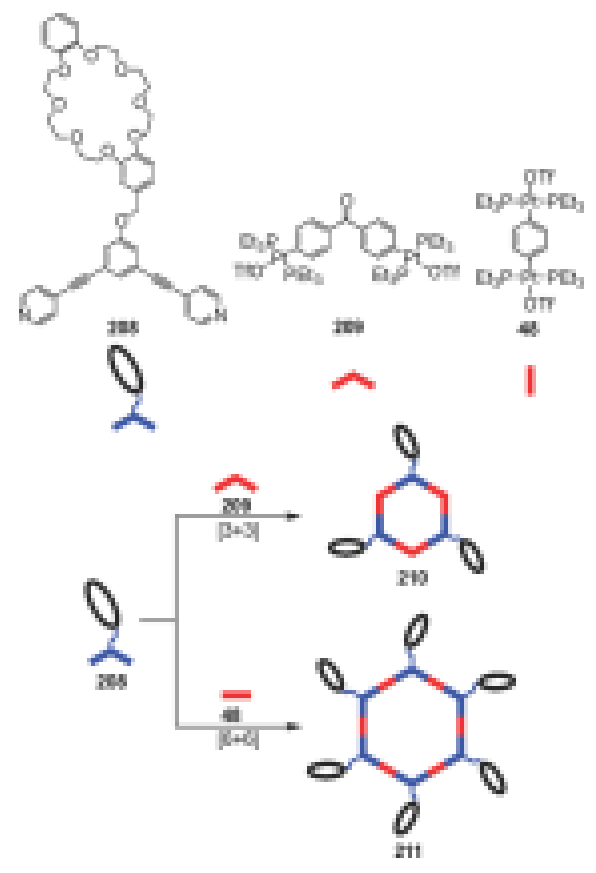
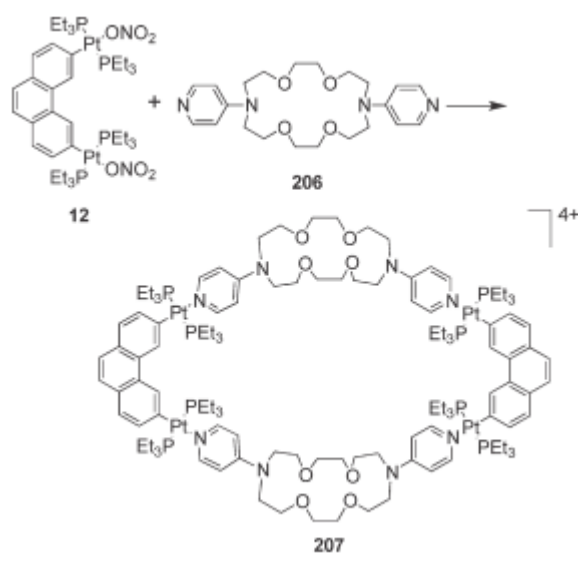
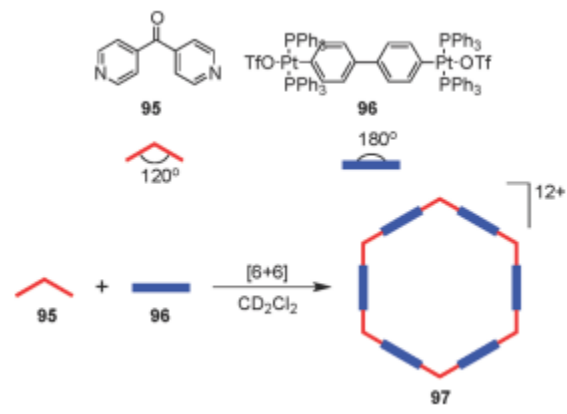


1

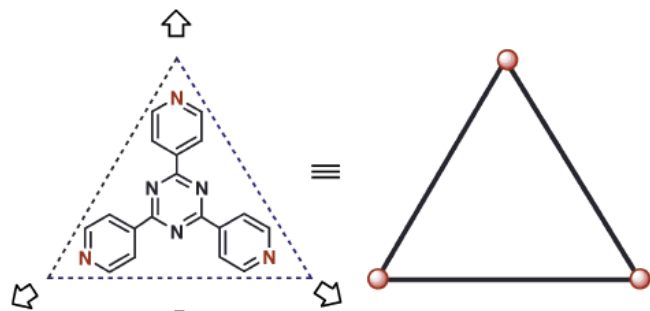
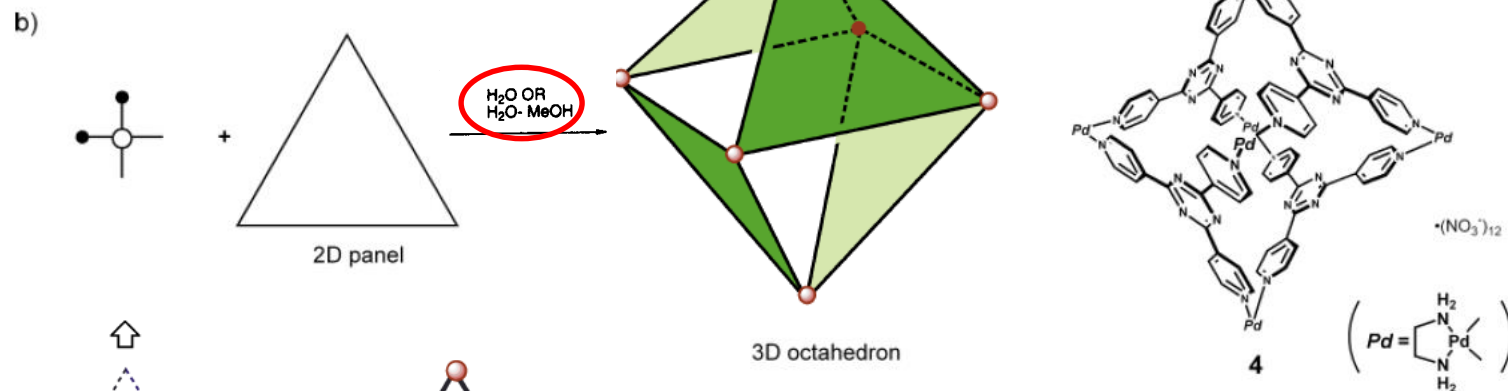
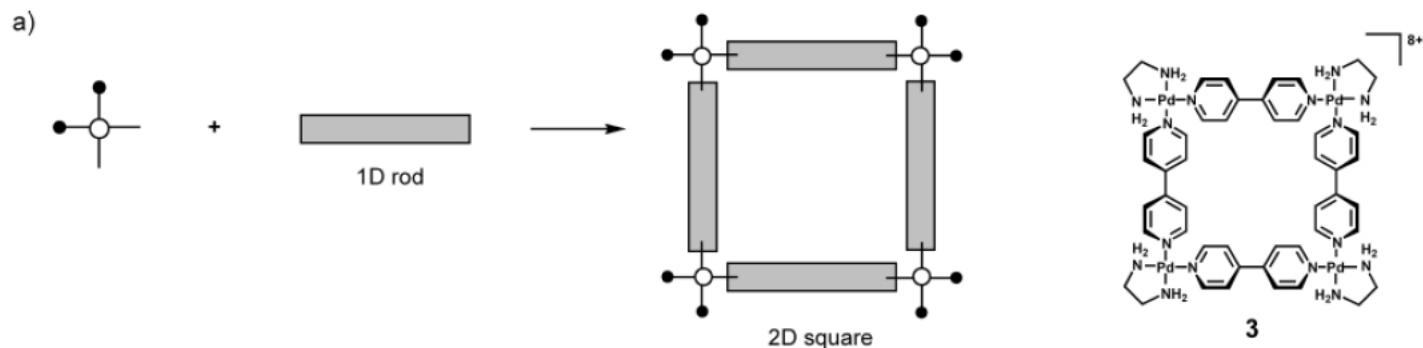
2



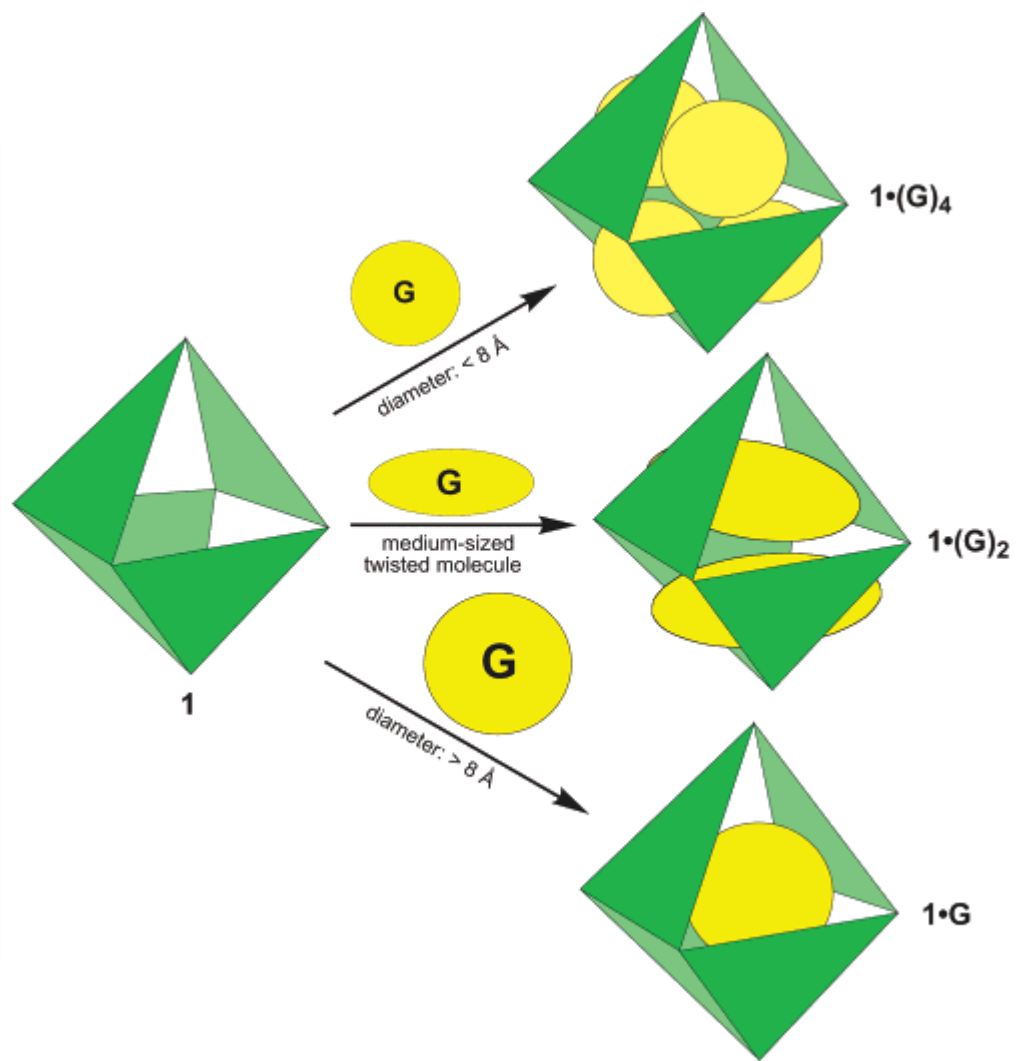
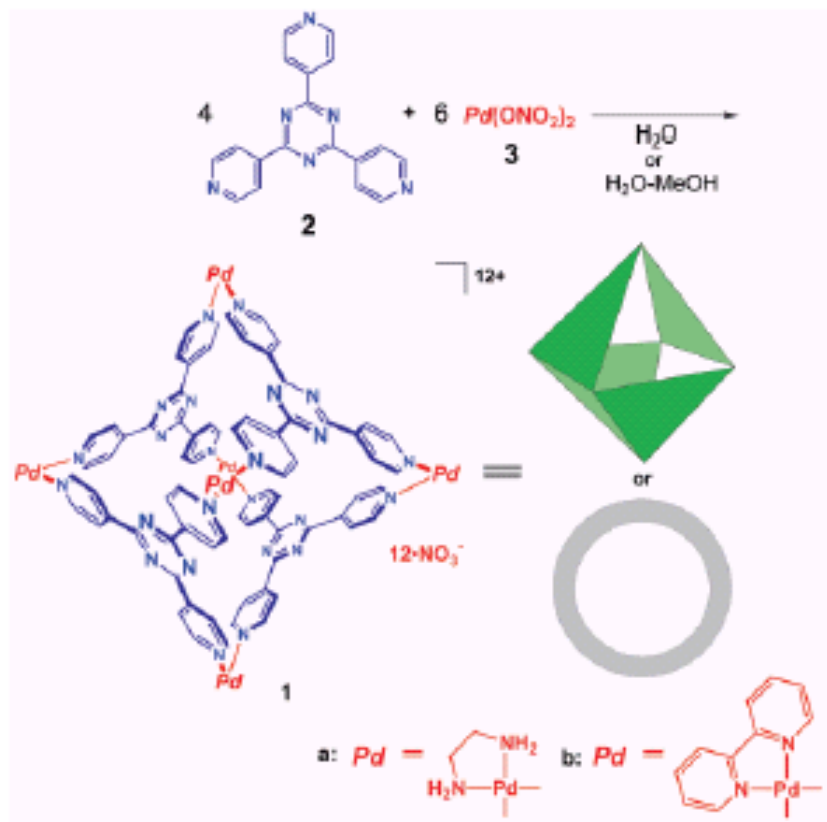




Makoto Fujita,* Kazuhiko Umemoto, Michito Yoshizawa, Norifumi Fujita, Takahiro Kusakawa and Kumar Biradha



M₆L₄
d ca. 11 Å
Portali 8 Å



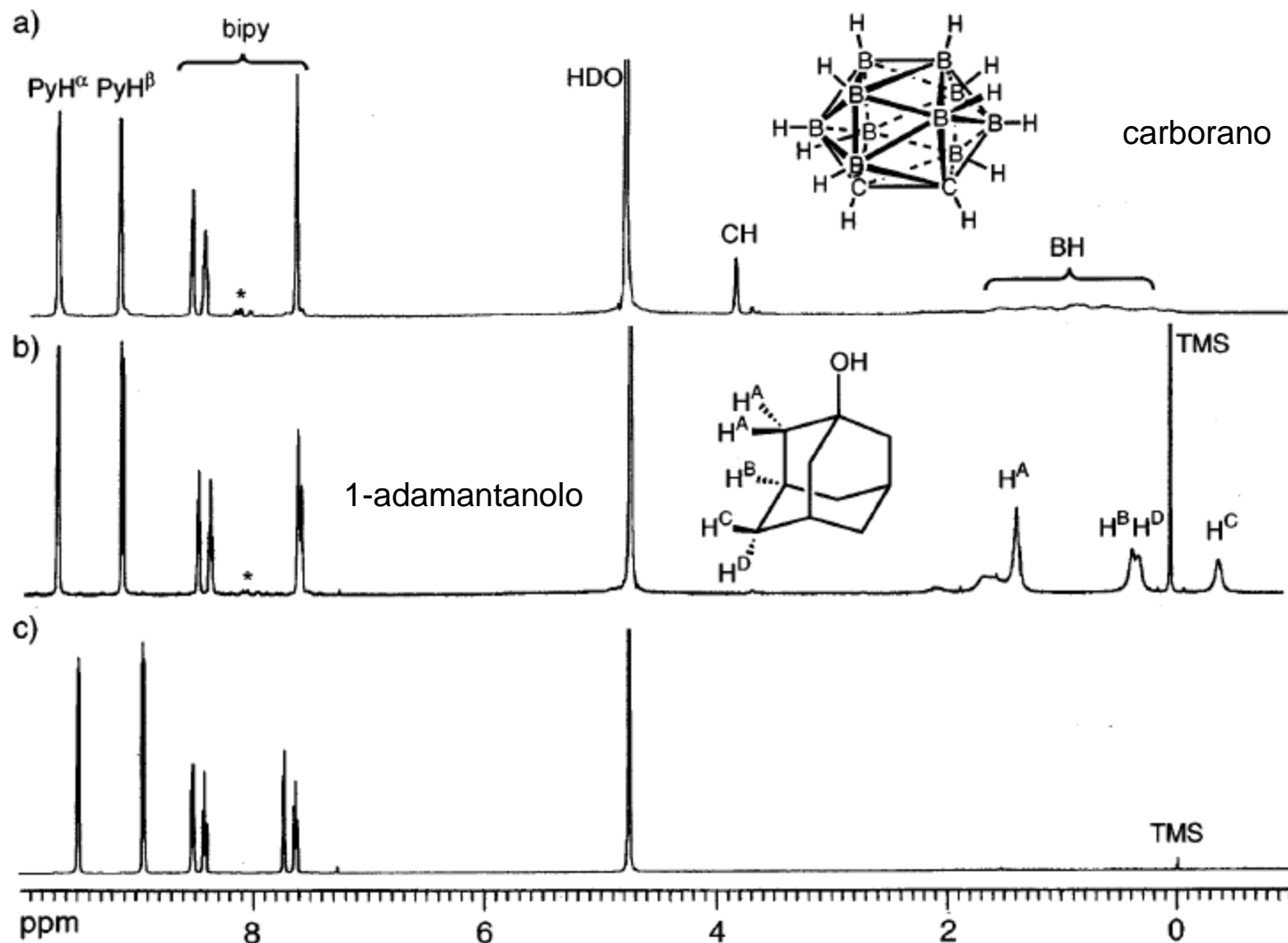
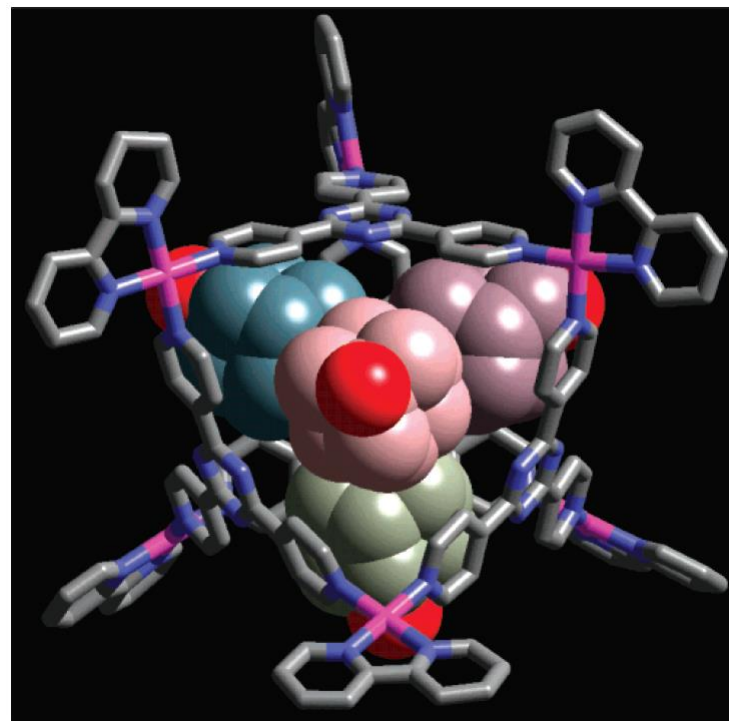
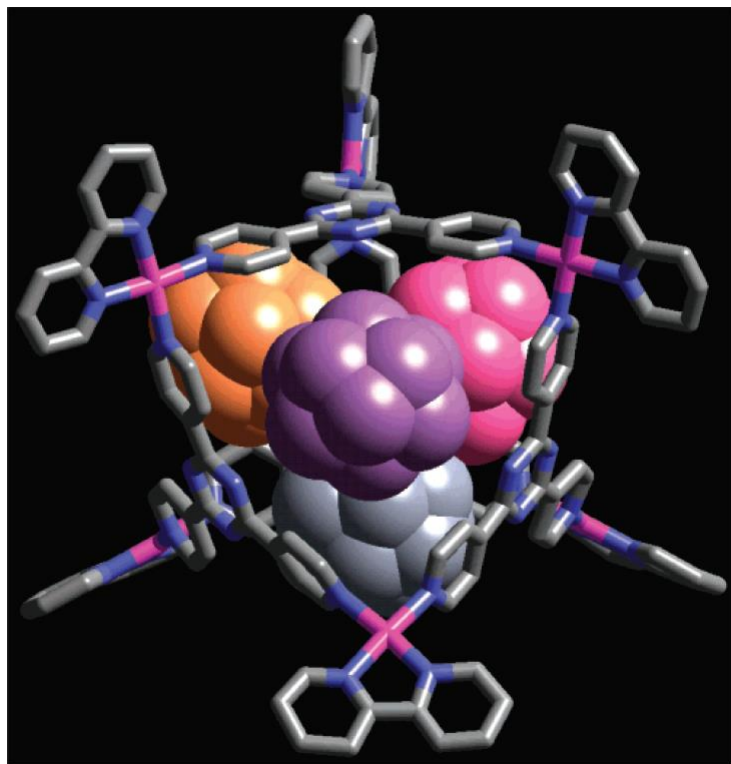
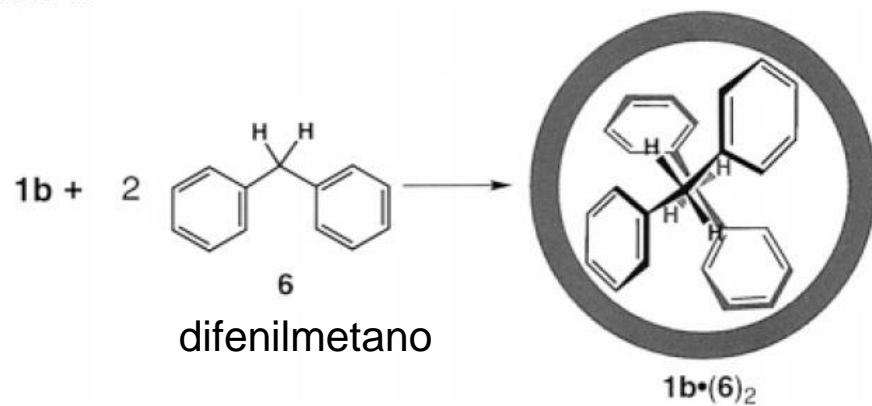


Figure 1. ^1H NMR observations of the enclathration of guest molecules in **1b**. (a) $1b \cdot (4)_4$. (b) $1b \cdot (5)_4$. (c) Empty **1b** (*: impurities).

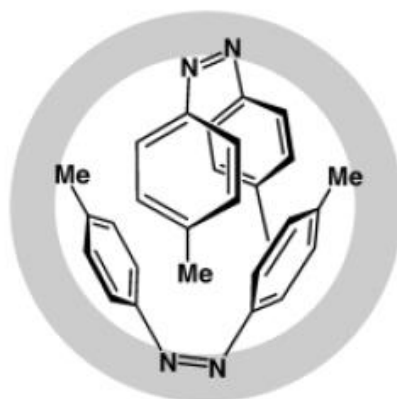


Scheme 2

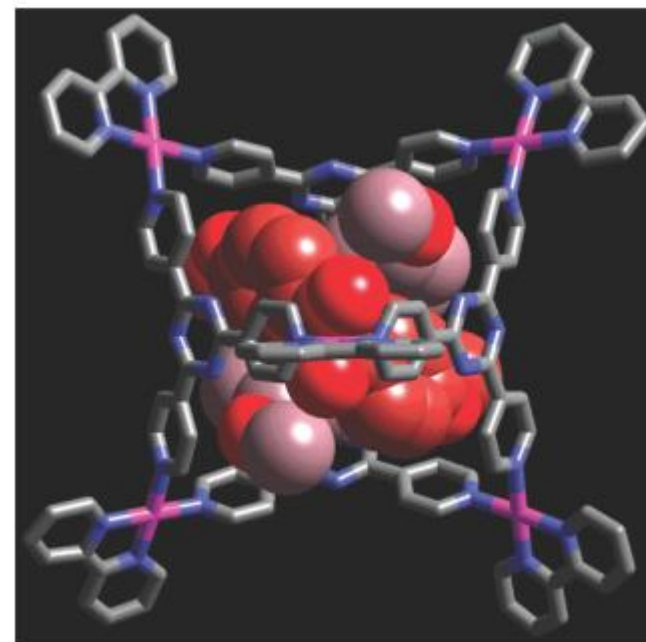
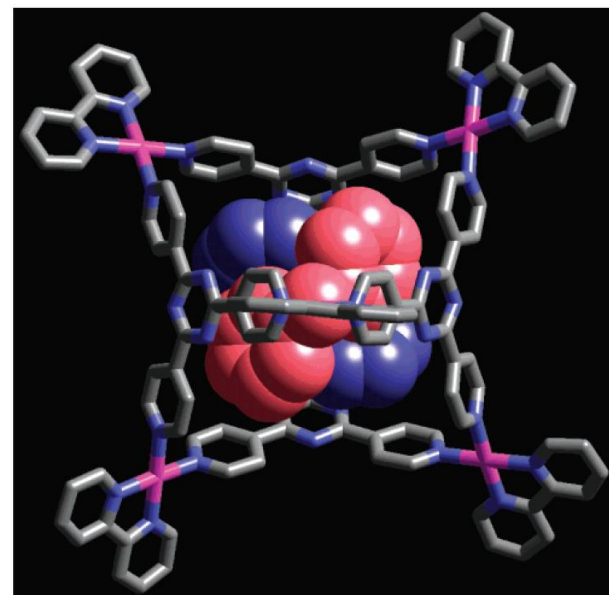
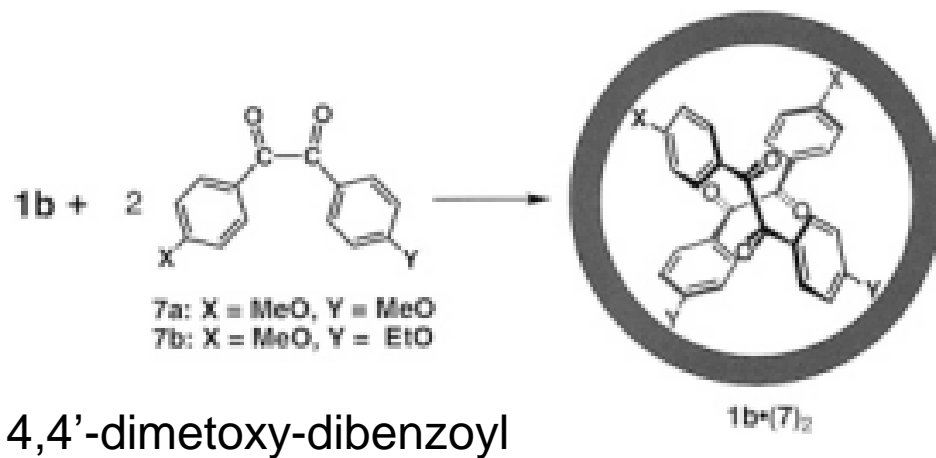


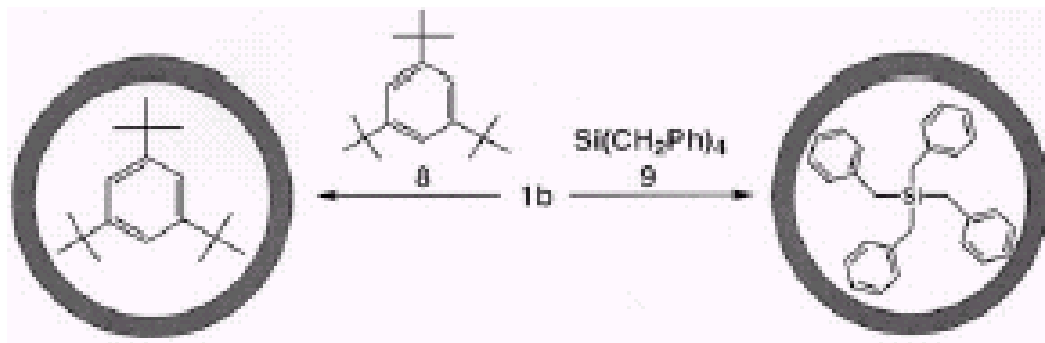
cis-azobenzene

cis-stylbene



Scheme 3





tri-*tert*-butylbenzene

tetrabenzylsilane

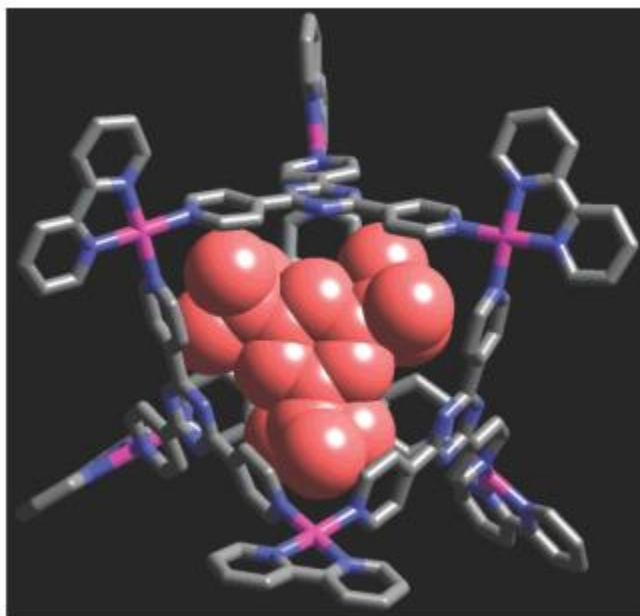
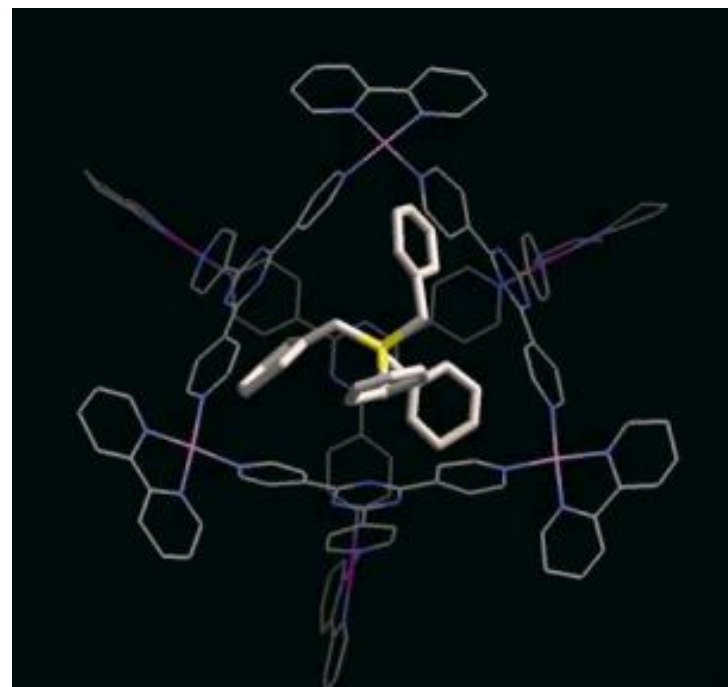
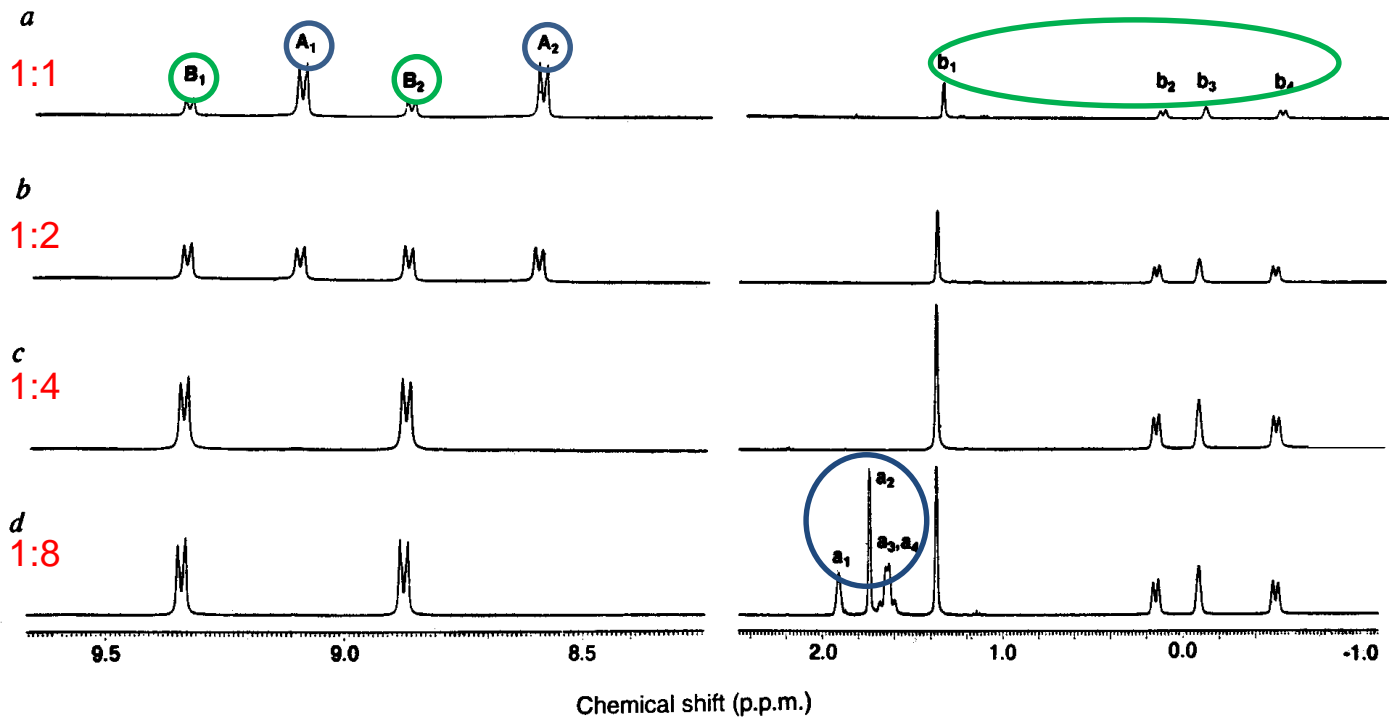


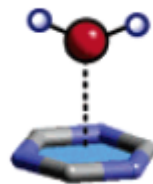
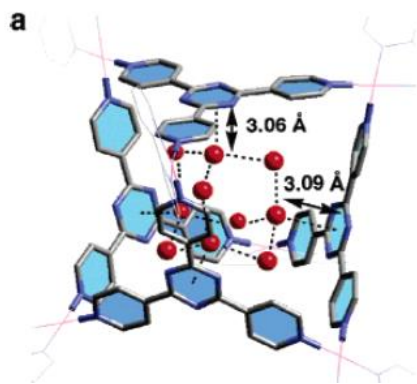
Figure 8. Crystal structure of 1b·8.

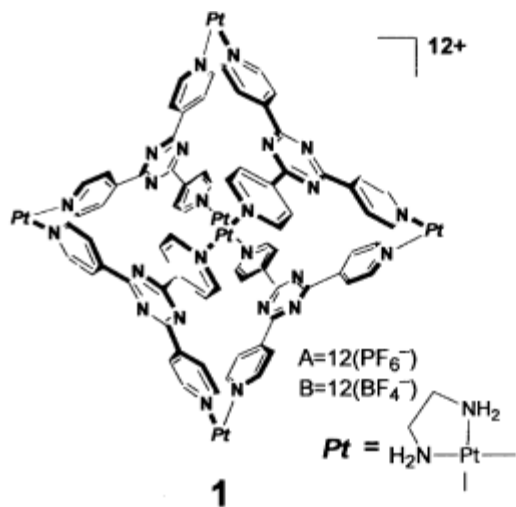




M_6L_4 /adamantancarboxylate₄

Allosteric effect!





a: (C₈₄H₉₆N₃₆Pt₆)¹²⁺•12(PF₆⁻)
FW. 4519.98

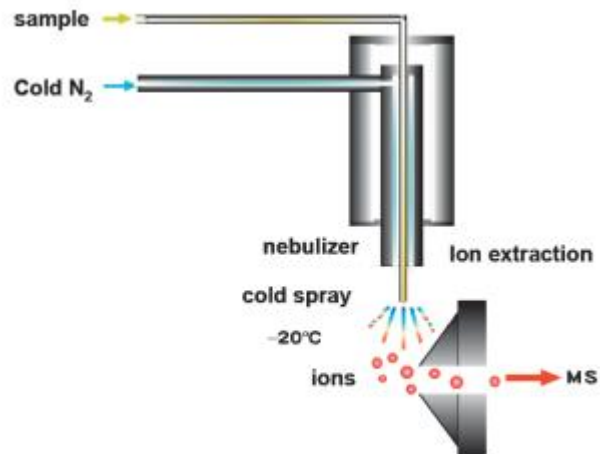


Fig. 1. Schematic illustration of the cold spray.

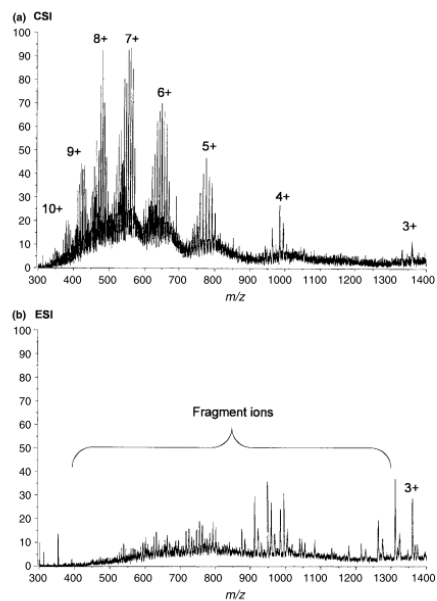
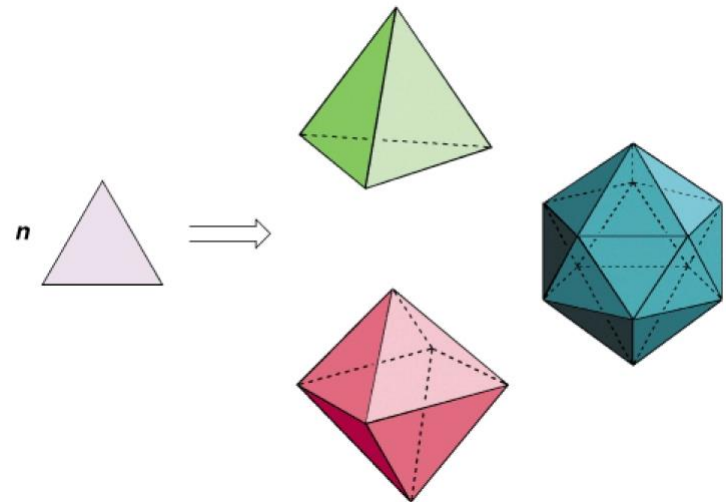
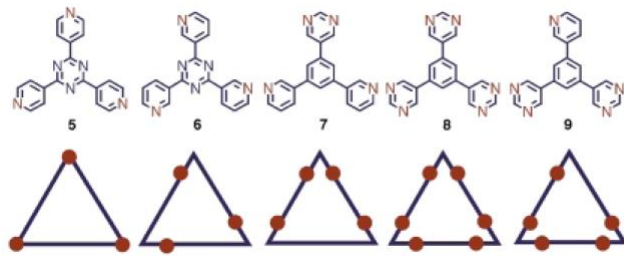
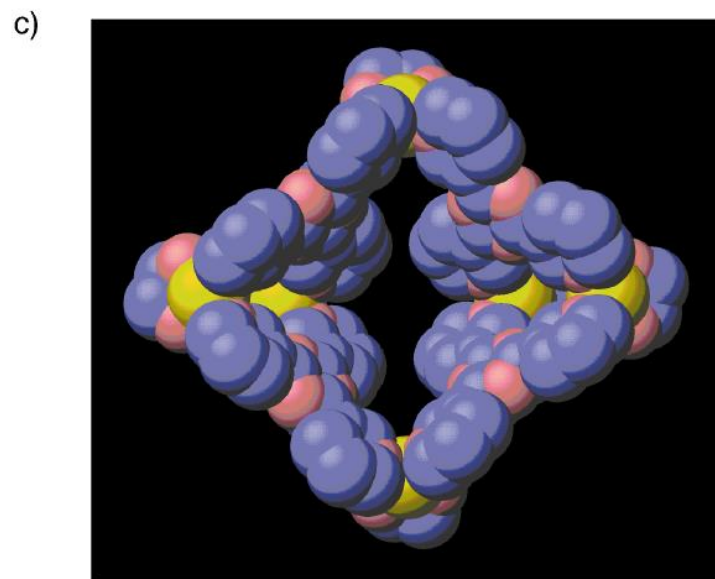
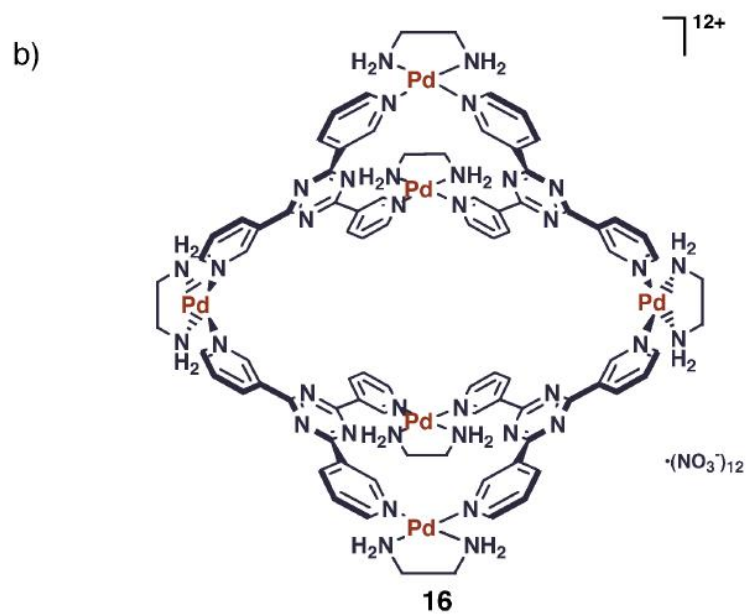
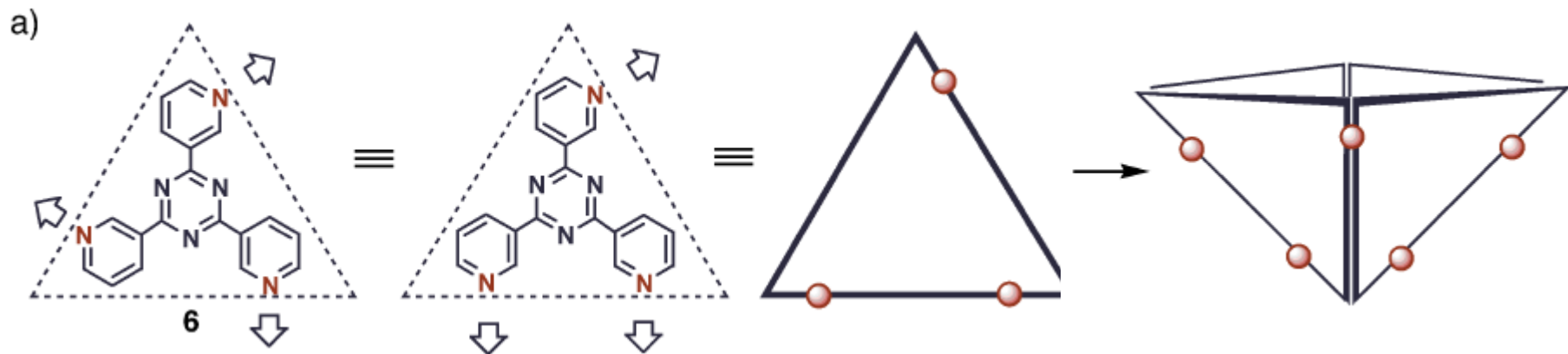


Figure 3. Comparison of (a) CSI and (b) ESI mass spectra of **1a**. Reprinted from Ref. 2 with permission from Elsevier.

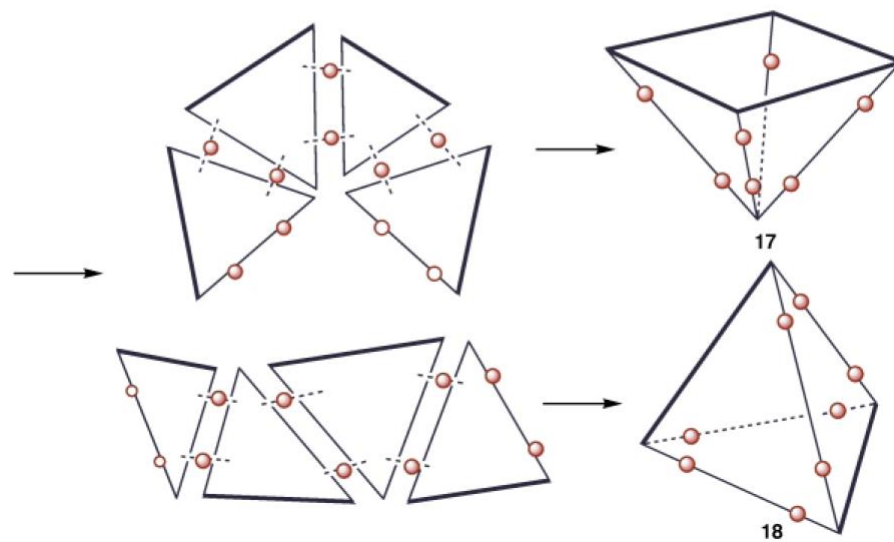
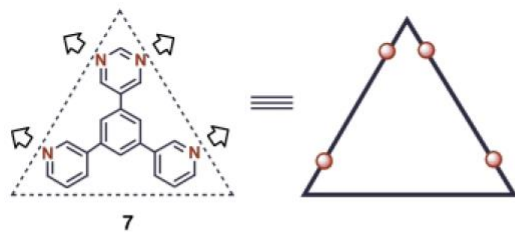
Molecular Paneling

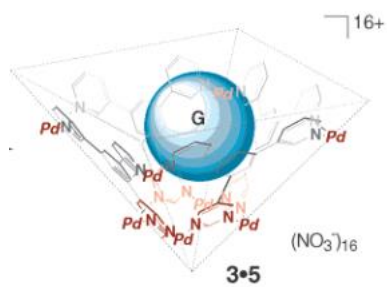
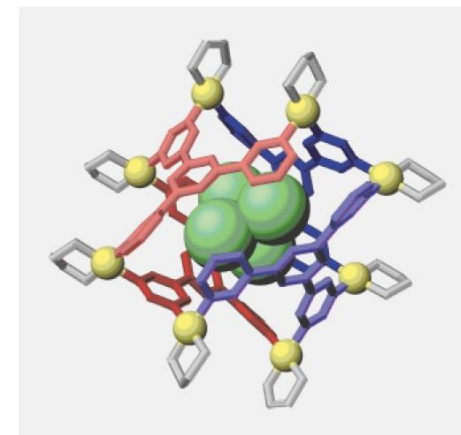
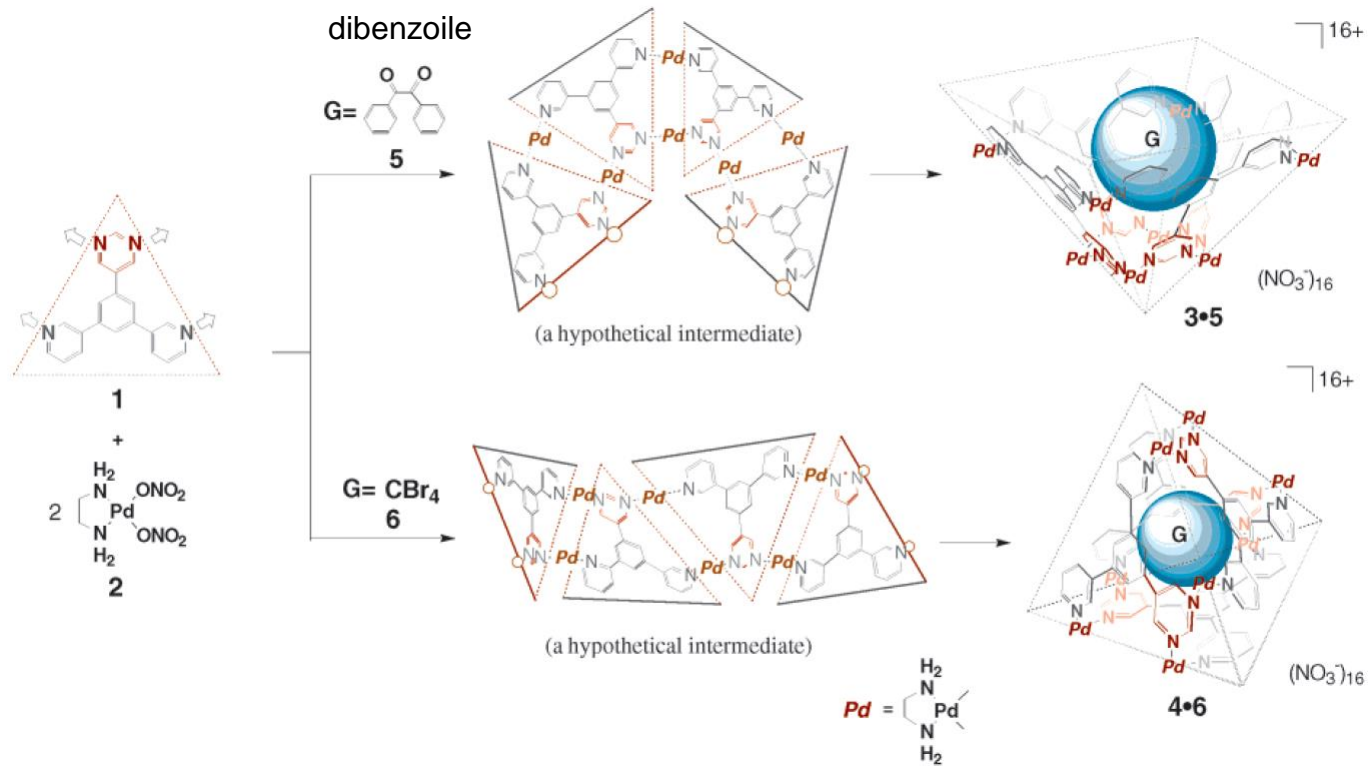
a)



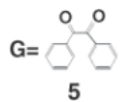
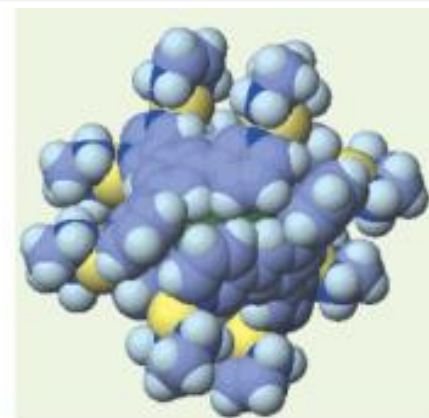
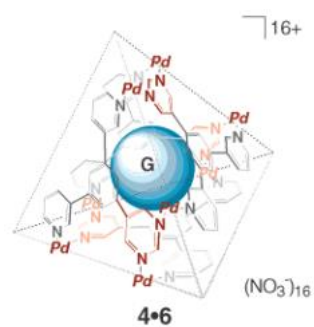
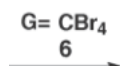


a)

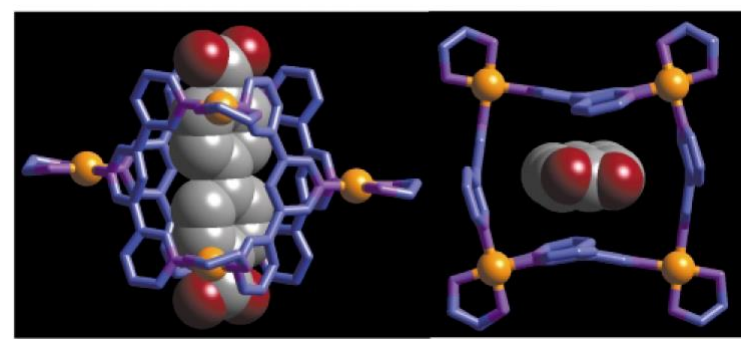
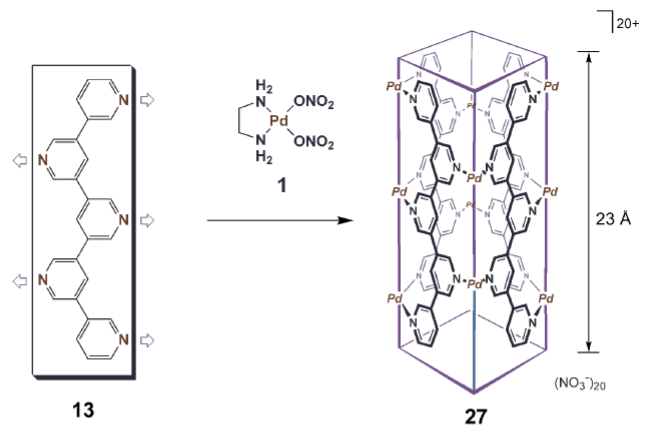




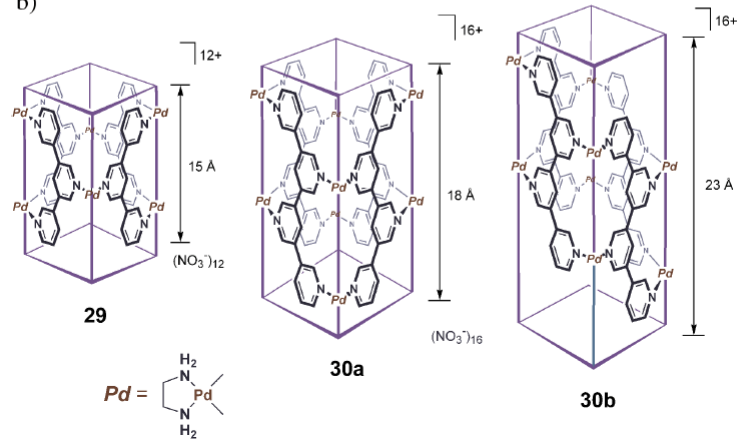
excess of



a)



b)



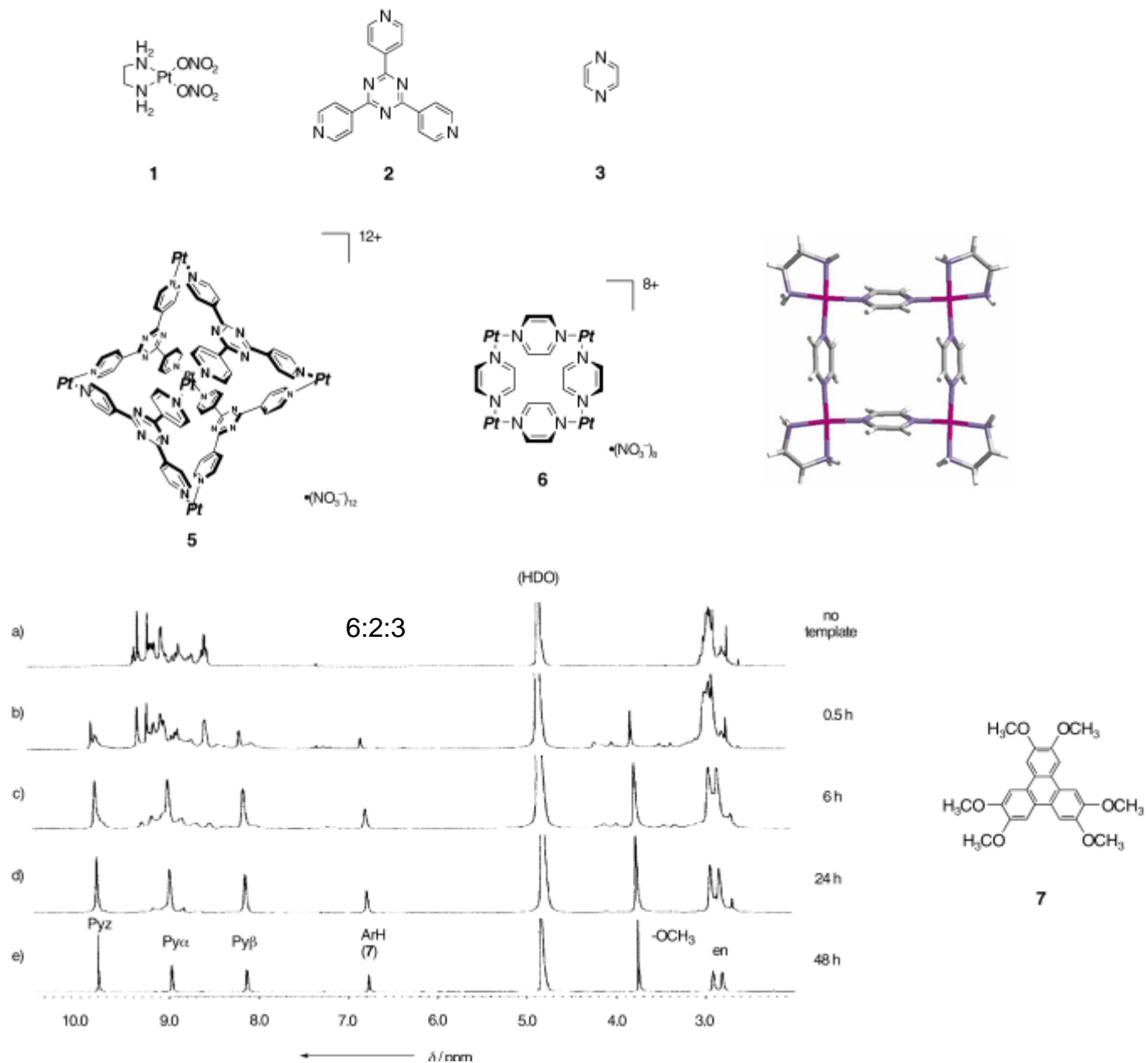
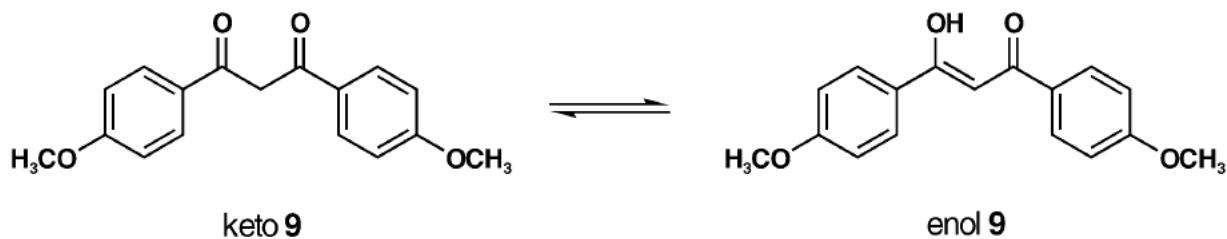
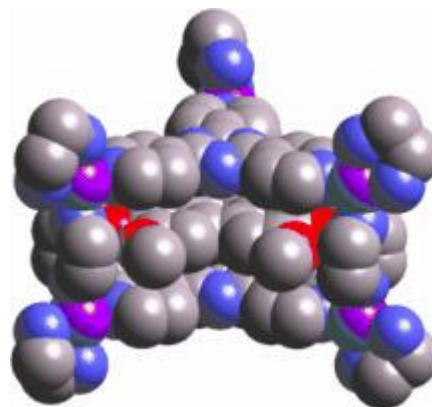
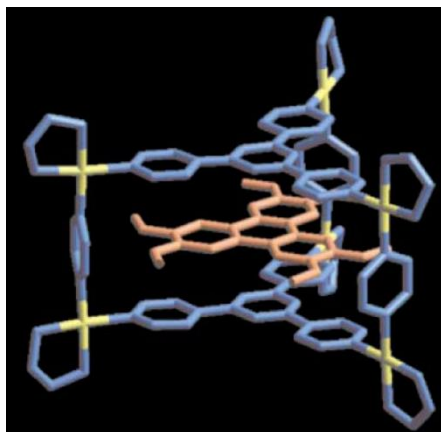


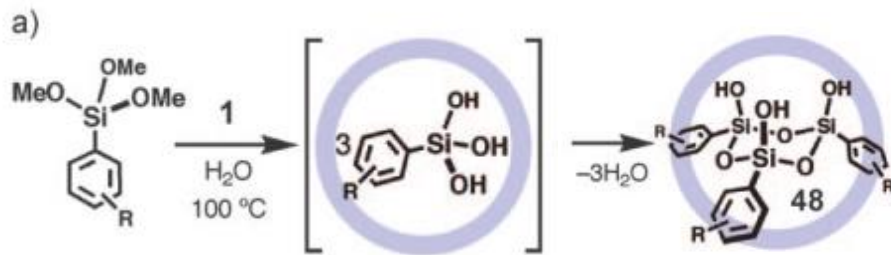
Figure 1. ¹H NMR spectra showing the guest-templated assembly of 7⊂4 complex (500 MHz, D₂O, 25 °C). a) A mixture of 1, 2, and 3. Template 7 was added to this solution and the mixture was heated at 100 °C for b) 0.5 h, c) 6 h, d) 24 h, and e) 48 h. Pyz = pyrazine.



The efficient intercalation of planar guest molecules within the cage was applied to the control of the equilibration between planer and nonplanar molecules. Keto and enol tautomers of β -diketone **9**, which exist in a 15:85 ratio in CD_3CN , can never be separated because of rapid tautomerization.

Stabilization of reactive intermediates: cyclic alcoxy-silanes

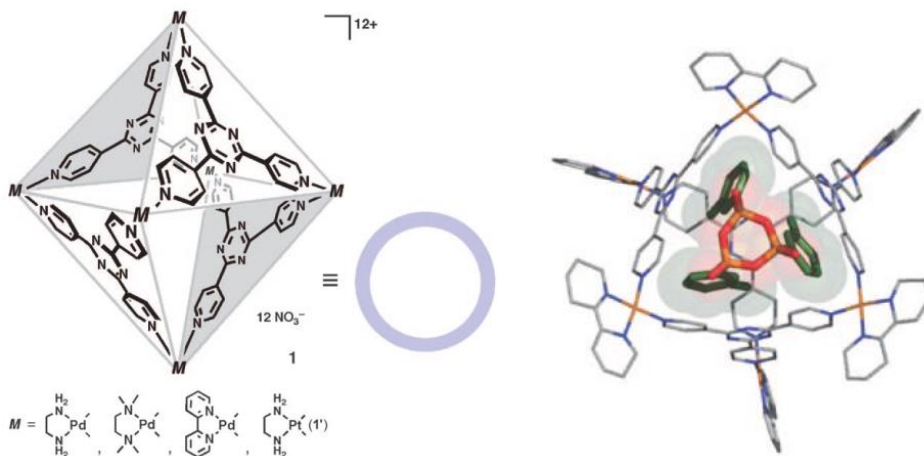
Ship in a Bottle



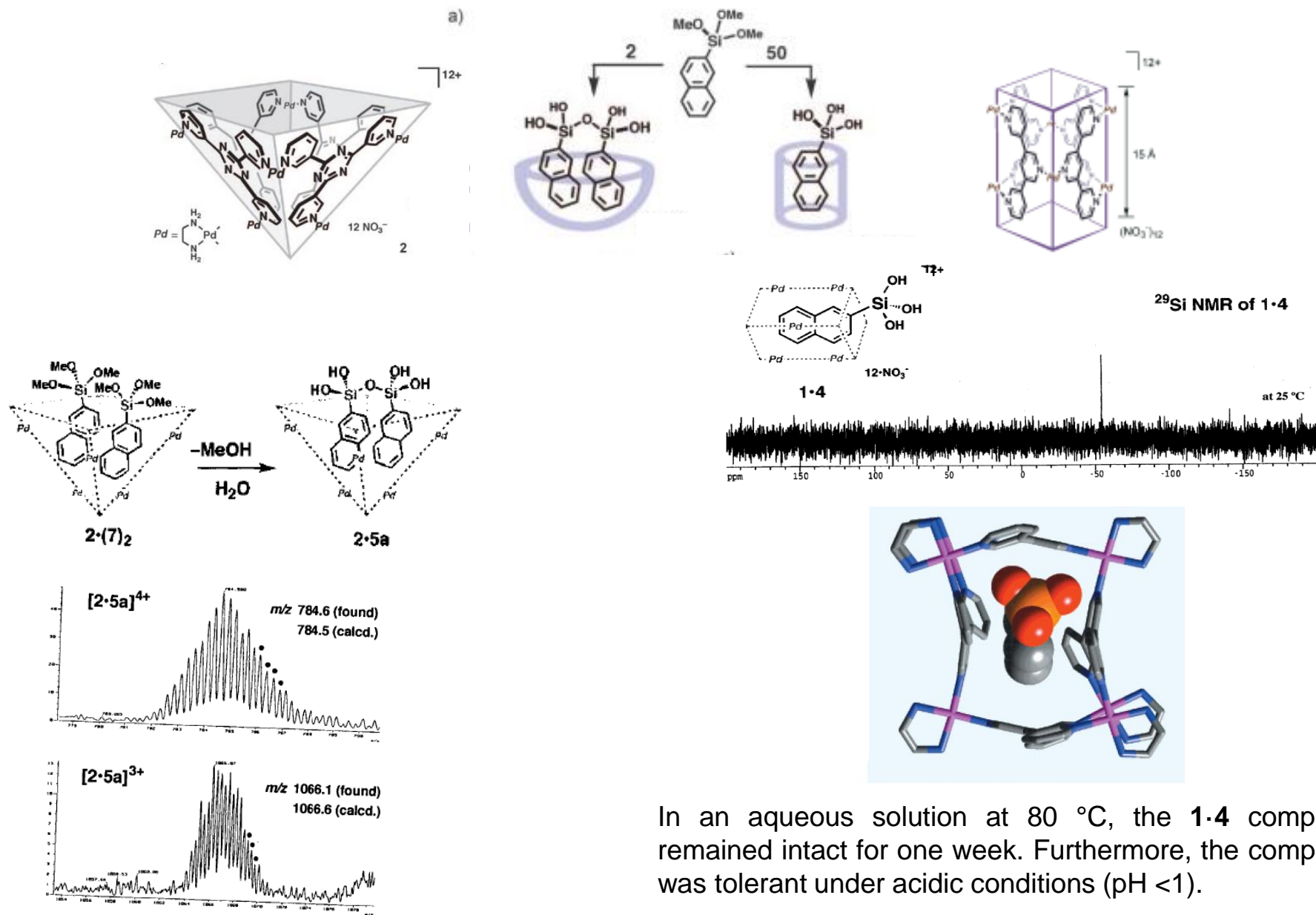
The roughly spherical cage cavity directs the selective formation of the cyclic trimer and prohibits further polycondensation despite the presence of labile Si-OH functional groups.

The stereochemistry of the condensation reaction is highly controlled within the cage giving only all-*cis* isomers.

The trimers prepared in situ can no longer escape from the cage because their dimension becomes larger than the portal size.



Stabilization of reactive intermediates: oligomerization of trialcoxy-silanes



Diels-Alder in Aqueous Molecular Hosts: Unusual Regioselectivity and Efficient Catalysis

Michito Yoshizawa, Masazumi Tamura, Makoto Fujita*

Science 2006;312:251-254

ERRATUM

Post date 9 June 2006

Reports: "Diels-Alder in aqueous molecular hosts: unusual regioselectivity and efficient catalysis" by M. Yoshizawa *et al.* (14 Apr. 2006, p. 251). Due to a nomenclature error, all references to "phthalimides" in the text and Supporting Online Material should instead refer to "maleimides." The chemical structures in the schemes and figures are all correct as drawn.

Fig. 1. Self-assembled coordination cages (1 and 2), which are prepared by simple mixing of an exo-tridentate organic ligand and an end-capped Pd(II) ion in a 4:6 ratio in water.

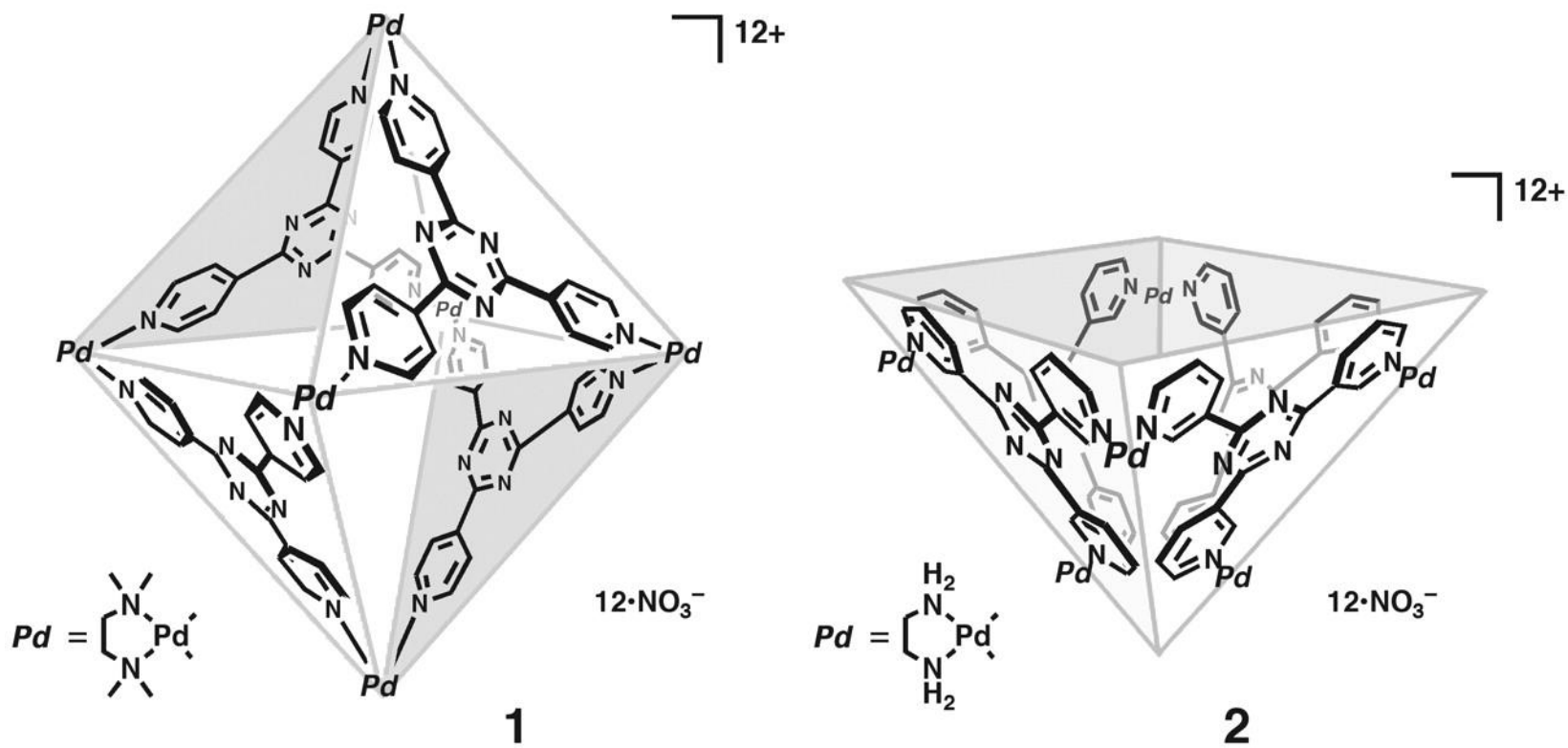
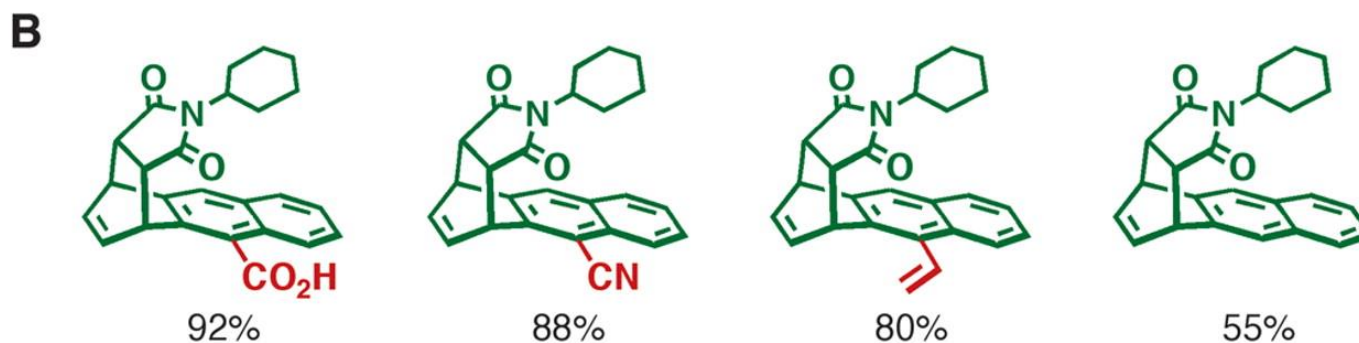
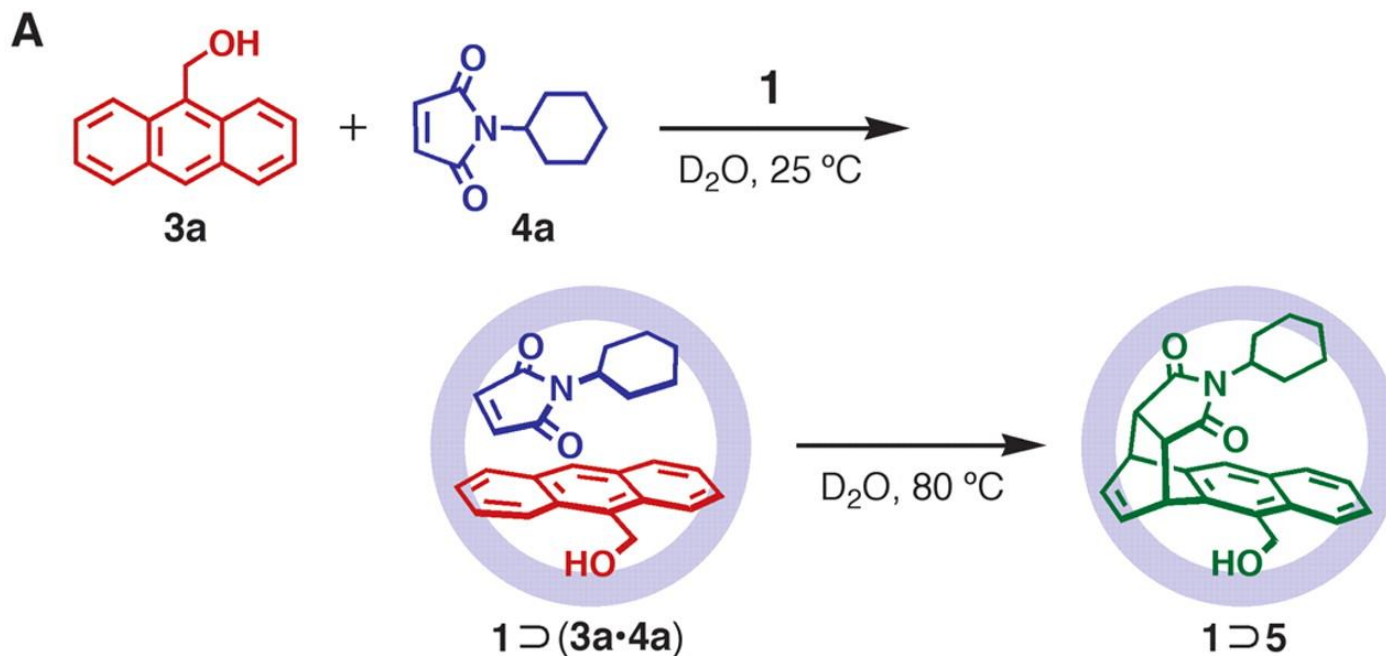


Fig. 2. (A) Pair-selective encapsulation of two types of reactants, 9-hydroxymethylanthracene (3a) and N-cyclohexylphthalimide (4a), within cage 1 and the subsequent Diels-Alder reaction leading to syn isomer of 1,4-adduct 5 within the cavity of 1.



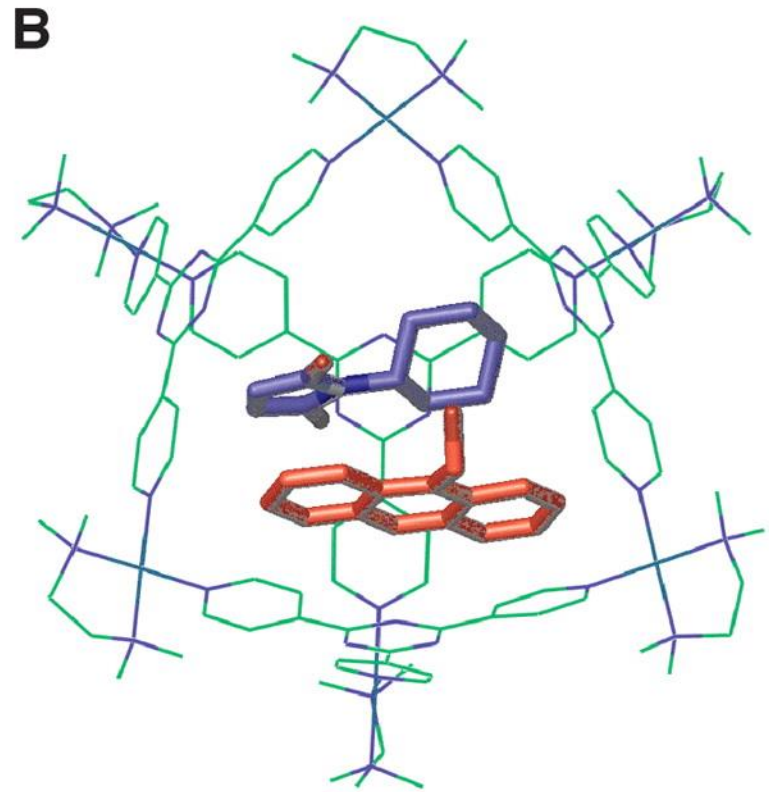
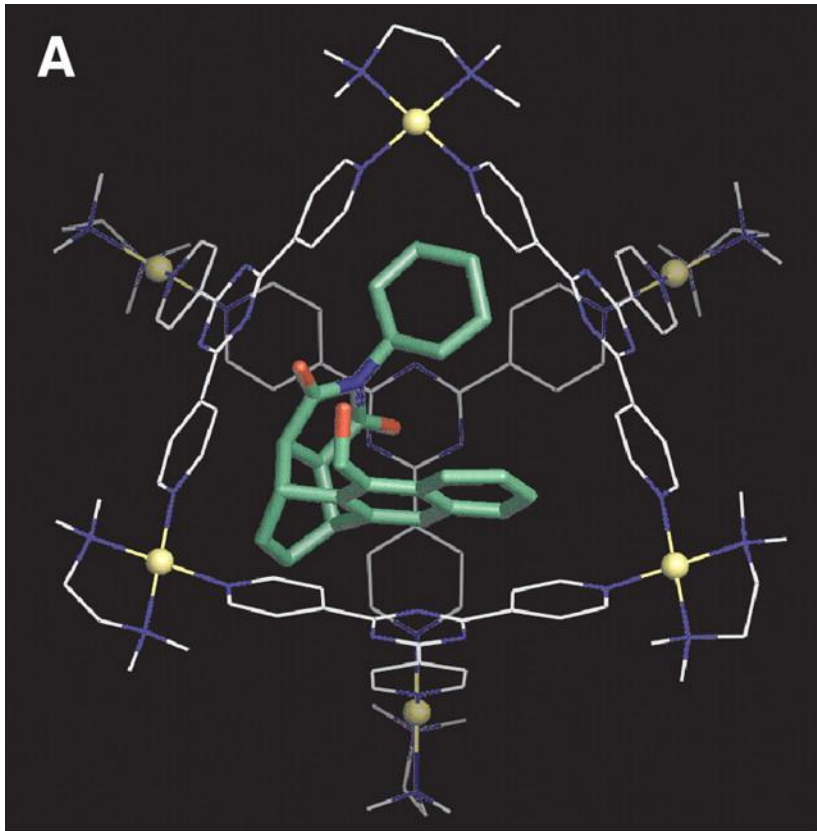


Fig. 4. Catalytic Diels-Alder reaction of 9-hydroxymethylantracene (3a) and N-phenylphthalimide (4c) in the aqueous solution of bowl 2, leading to 9,10-adduct 6.

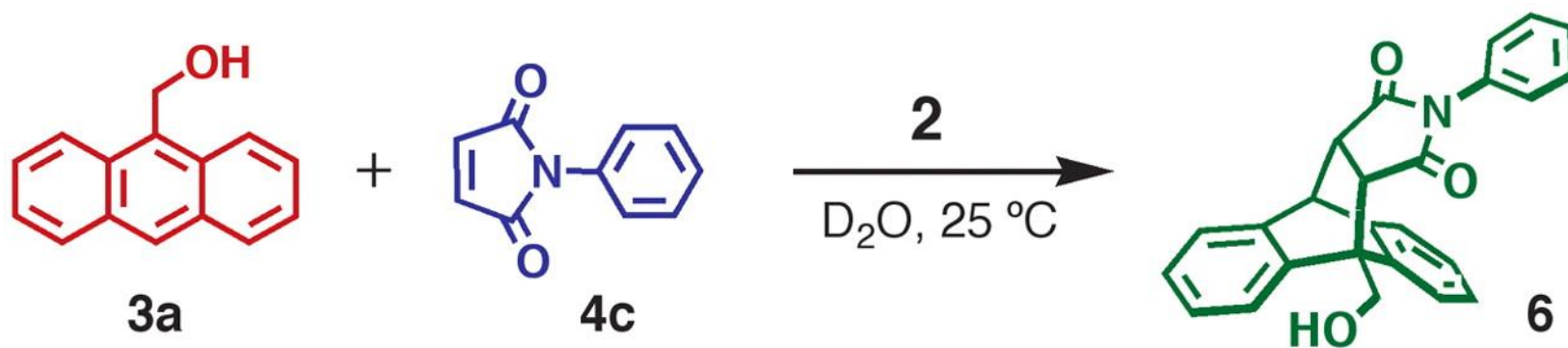


Fig. 5. The ^1H NMR spectra (500 MHz, room temperature) of the catalytic Diels-Alder reaction of 9-hydroxymethylantracene (3a) and N-phenylphthalimide (4c) in an aqueous solution of bowl 2.

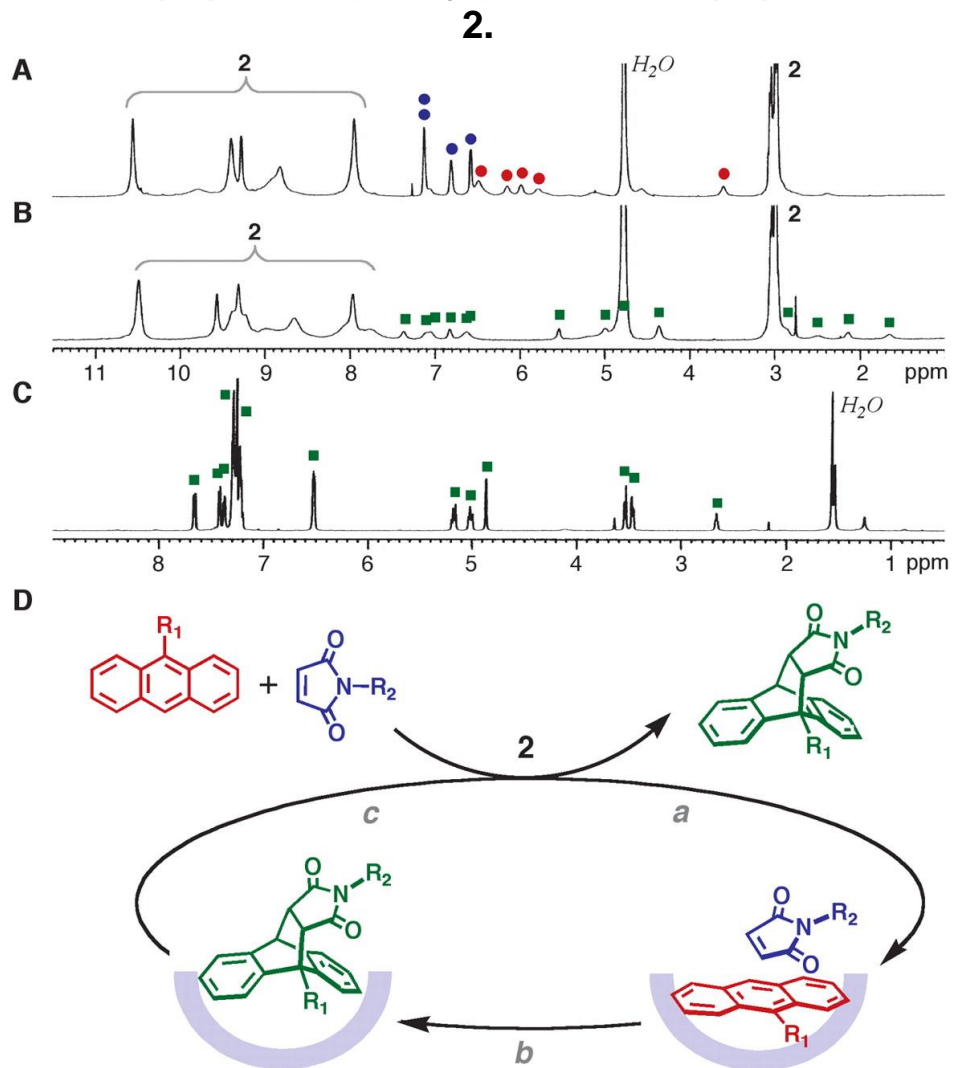
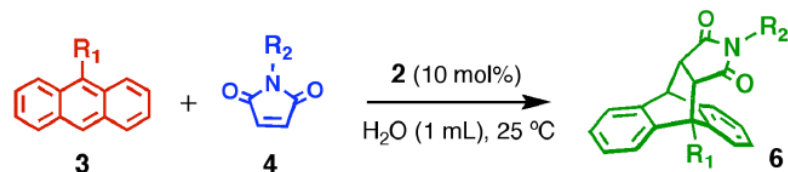
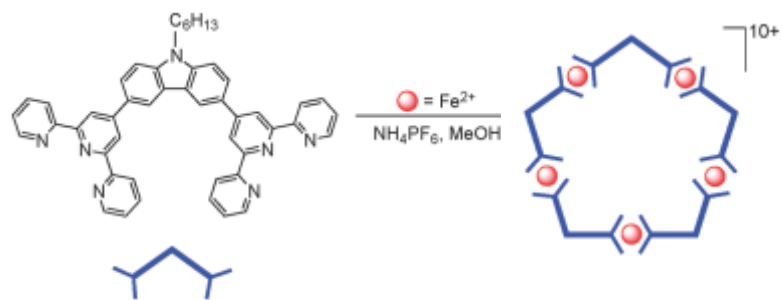
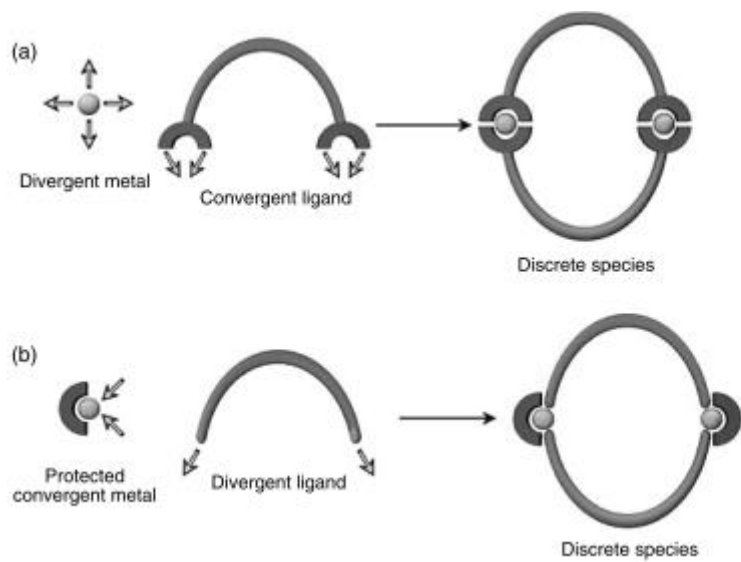


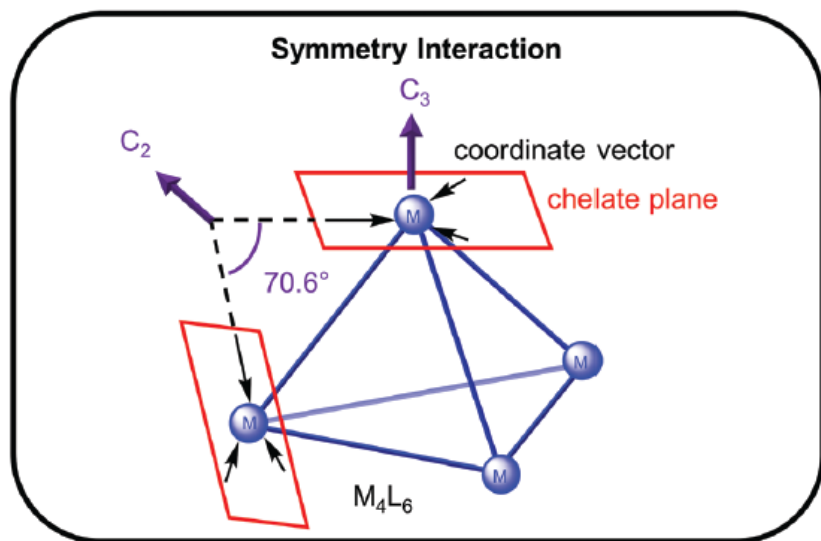
Table S1. Catalytic Diels-Alder reaction of **3** and **4** in the presence of **2** (10 mol%) in H₂O (1 mL) and control experiments in H₂O or CDCl₃ (1 mL) without **2**.



Entry	Substrate		Time	Yield(%) of 6		
	3 (R ₁)	4 (R ₂)		with 2	without 2	in CHCl ₃ [†]
1	-CH ₂ OH	propyl	5 h	>99	8	0
2	-CH ₂ OH	cyclohexyl	15 h	98	0	6
3	-CH ₂ OH	phenyl	5 h	>99 ^{*,†}	3	9
4	-CH ₂ OH	phenyl	15 h	6	7	21
5	-CH ₂ OH	benzyl	5 h	>99	trace	0
6	-CH ₂ OH	xylyl	15 h	94	0	17
7	-CH ₃	cyclohexyl	7 h	>99	0	5
8	-CH ₃	phenyl	3 h	>99	5	17
9	-CH=CH ₂	phenyl	1 d	88	0	trace
10	-CH=CH ₂	benzyl	1 d	97	5	4
11	-CO ₂ H	benzyl	1 d	12	0	0
12	-CH ₂ OH	phenyl	1 d	>99 [‡]	—	—

^{*}(en)Pd(NO₃)₂: 10 mol% [†]without **2** [‡]**2** : 1 mol%, hexane (1 mL)





Supramolecules by Design

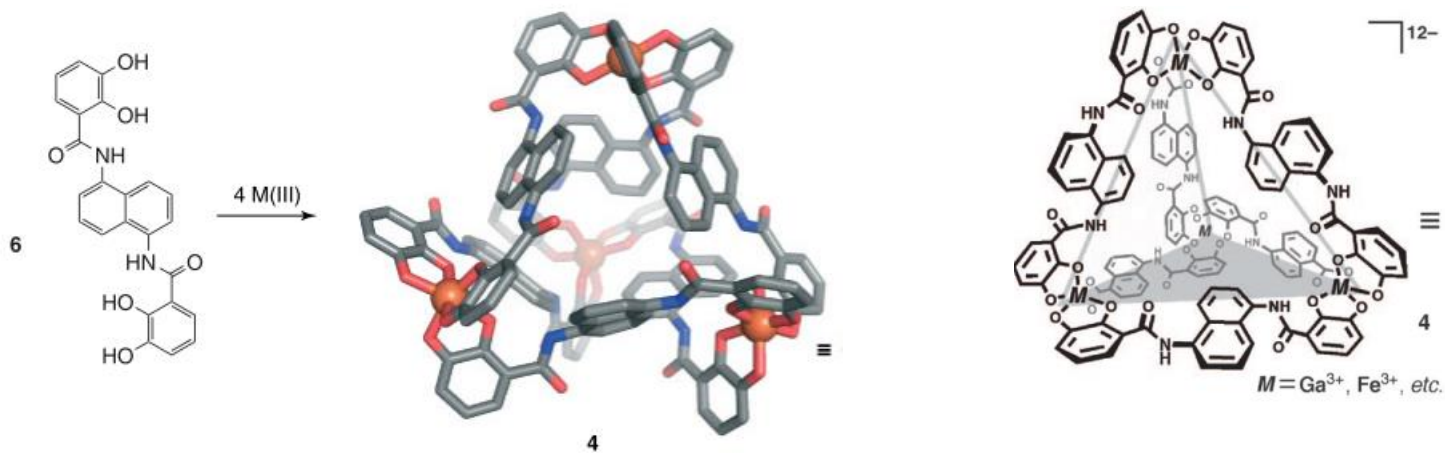
DANA L. CAULDER AND
KENNETH N. RAYMOND*

Acc. Chem. Res. **1999**, *32*, 975–982

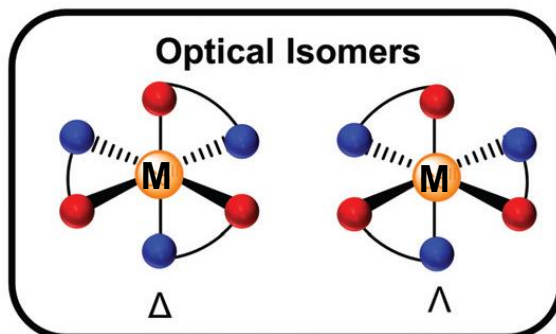
J. Am. Chem. Soc. **2001**, *123*, 8923–8938

Design, Formation and Properties of Tetrahedral M_4L_4 and M_4L_6
Supramolecular Clusters¹

Dana L. Caulder, Christian Brückner, Ryan E. Powers, Stefan König, Tatjana N. Parac,
Julie A. Leary, and Kenneth N. Raymond*



M_4L_6 , (Ga^{3+} , Fe^{3+} ; biscatechol-amides) 12^- , $\Delta\Delta\Delta\Delta$, $\Lambda\Lambda\Lambda\Lambda$, 300-350 Å
 Stabilization of organic cations



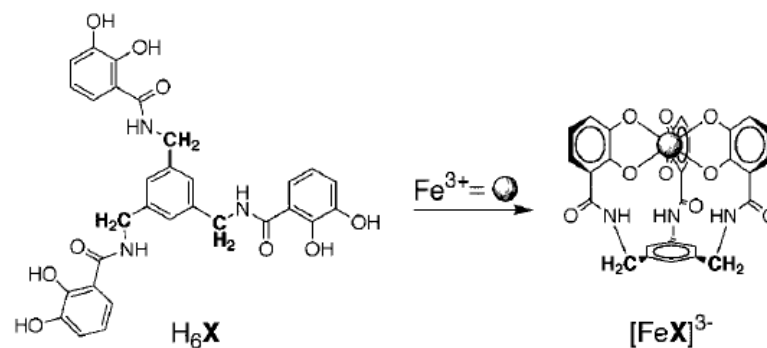
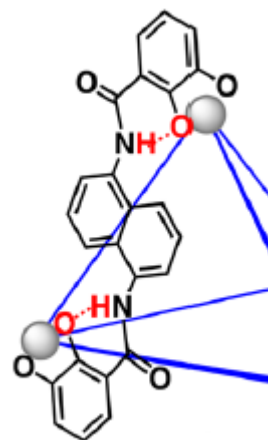
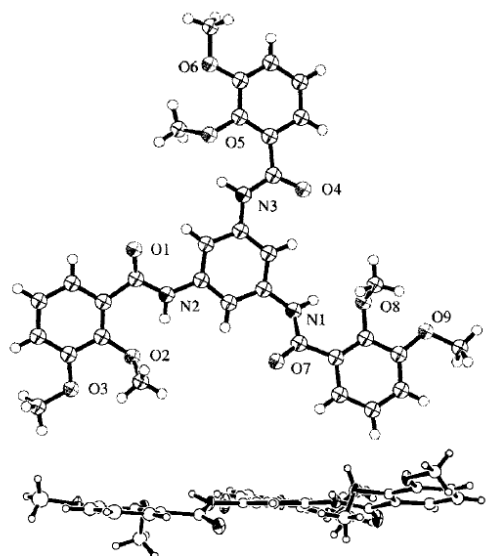


Figure 4. As shown in the enterobactin analogue H_6X , simple addition of a methylene group between the three-fold benzene scaffold and the catecholamide binding units gives the ligand enough flexibility to allow each of the arms to coordinate a single metal ion. This type of ligand flexibility must be avoided if multimetal clusters are desired.

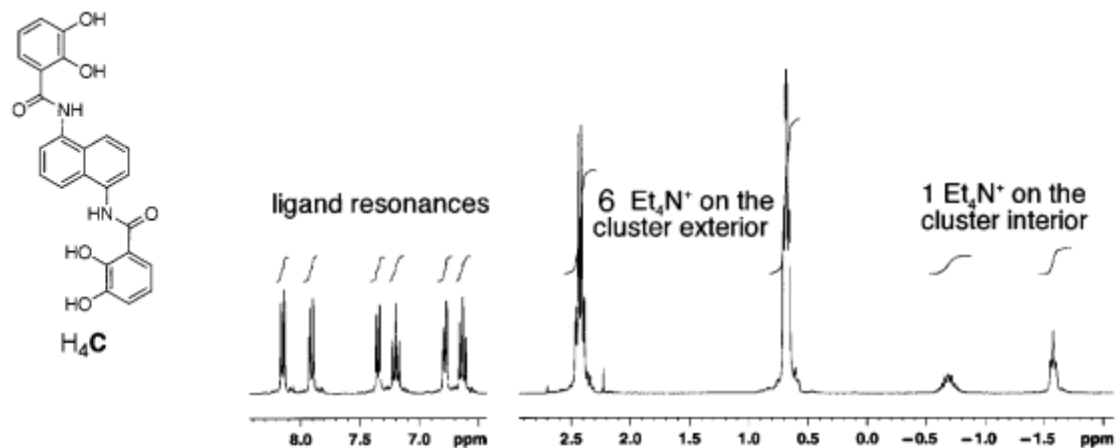


Figure 14. ^1H NMR (D_2O) depicting the two sets of Et_4N^+ resonances characteristic of the exterior and encapsulated cations.

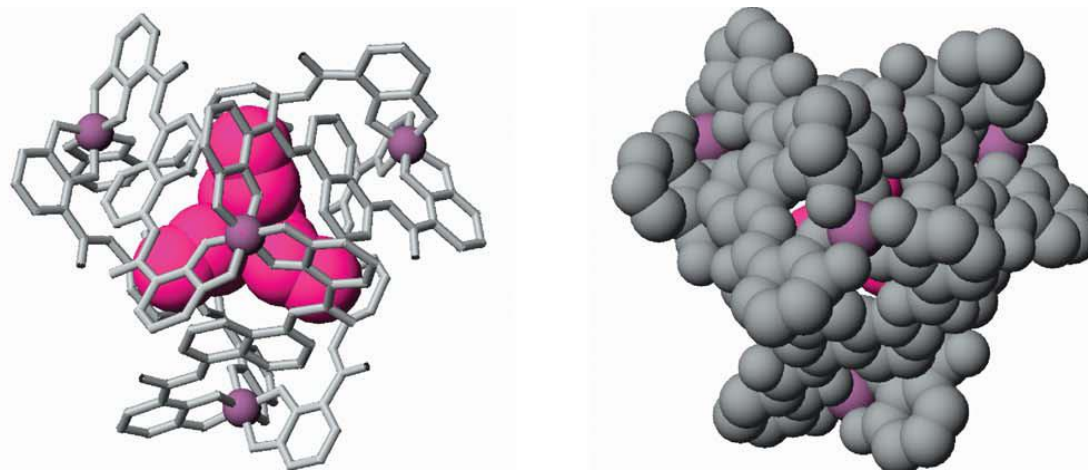
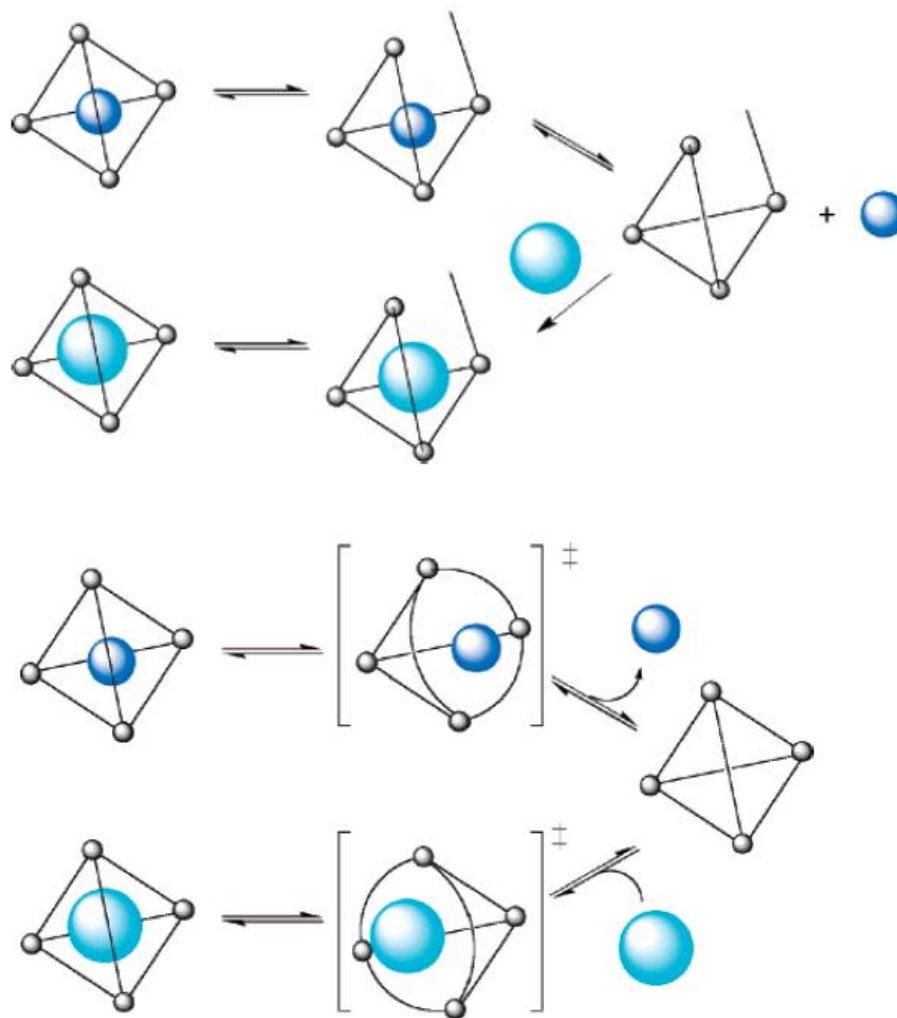
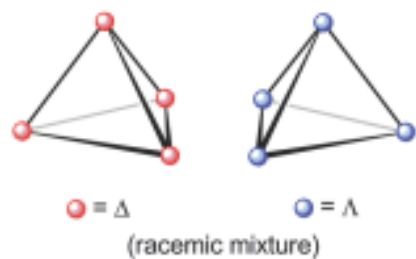


Figure 15. Based on the X-ray structure coordinates, $\text{Et}_4\text{N}^+ \text{C}[\text{Fe}_4\text{C}_6]^{12-}$ in both (a) wire-frame and (b) space-filling representations.

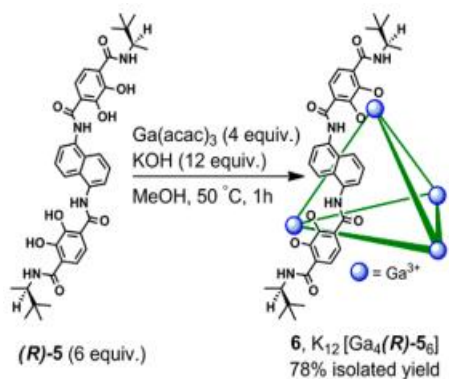
ESI-MS data

Guest exchange in an M_4L_6 supramolecular host has been evaluated to determine whether host rupture is required for guest ingress and egress. Two mechanistic models were evaluated: one requiring partial dissociation of the host structure to create a portal for guest passage and one necessitating deformation of the host structure to create a dilated aperture for guest passage without host rupture.





Resolution of the racemate using (-)-N'-methylnicotinium iodide: enantiopure $\Lambda\Lambda\Lambda\Lambda$ -(S-nic c cage) and $\Delta\Delta\Delta\Delta$ -(S-nic c cage) stereoisomers, after sequential ion exchange chromatography.



Achieving enantiopure M_4L_6 assembly without resolution using an amide-containing chiral directing group at the vertex of ligand - (*R*)-5 OR (*S*)-5.

$\mathbf{6}\text{-K}_{12}\text{Ga}_4(R)\text{-}5_6$ and $\mathbf{6}\text{-K}_{12}\text{Ga}_4(R)\text{-}5_6$ by CD spectroscopy: similar to those of $\Delta\Delta\Delta\Delta$ -cage and $\Lambda\Lambda\Lambda\Lambda$ -cage from racemate resolution.

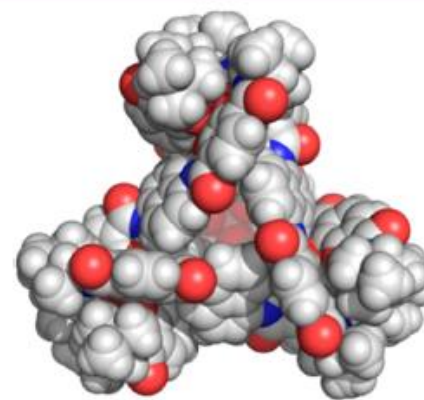
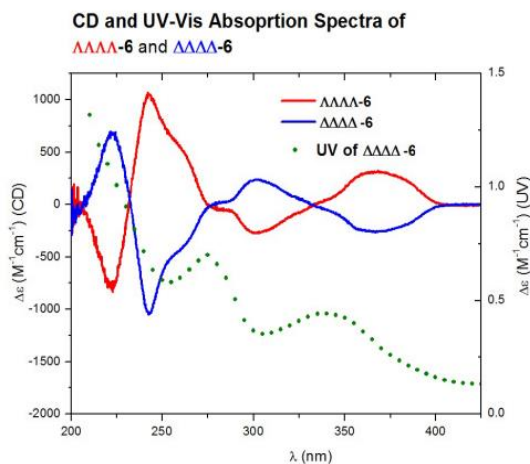
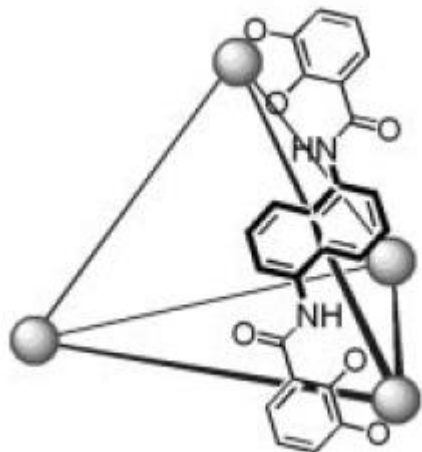


Figure 2. X-ray structure of $\Delta\Delta\Delta\Delta\text{-}6$.



4

Addition of one equivalent of **4** to the $[\text{Ga}_4\text{L}_6]^{12-}$ assembly in D_2O results in the shift of the tropylium singlet from $\delta = 6.45$ to 2.95 ppm (Figure 4, a). Integration of this upfield-shifted tropylium signal indicates that this cation is encapsulated as a guest inside the tetrahedral assembly with a 1:1 ratio. Addition of a second equivalent of tropylium ion results in a second broad resonance at $\delta = 5.18$ ppm (Figure 4, b). The upfield shift of this resonance, compared to the resonance of free tropylium in D_2O , indicates that the second equivalent of aromatic tropylium cation interacts with the $[\text{Ga}_4\text{L}_6]^{12-}$ assembly by ion-pair association with the highly-charged assembly, as seen

After 20 h in solution (Figure 4, c), the encapsulated tropylium signal is still sharp, while the signal for the tropylium associated with the assembly was noticeably broadened, and the signal for free tropylium at $\delta = 6.45$ ppm is unobservable. Free tropylium completely decomposes in D_2O after approximately 24 h, so it seems that encapsulation of this cation in the hydrophobic environment of the $[\text{Ga}_4\text{L}_6]^{12-}$ cavity has significantly increased its stability.^[26]

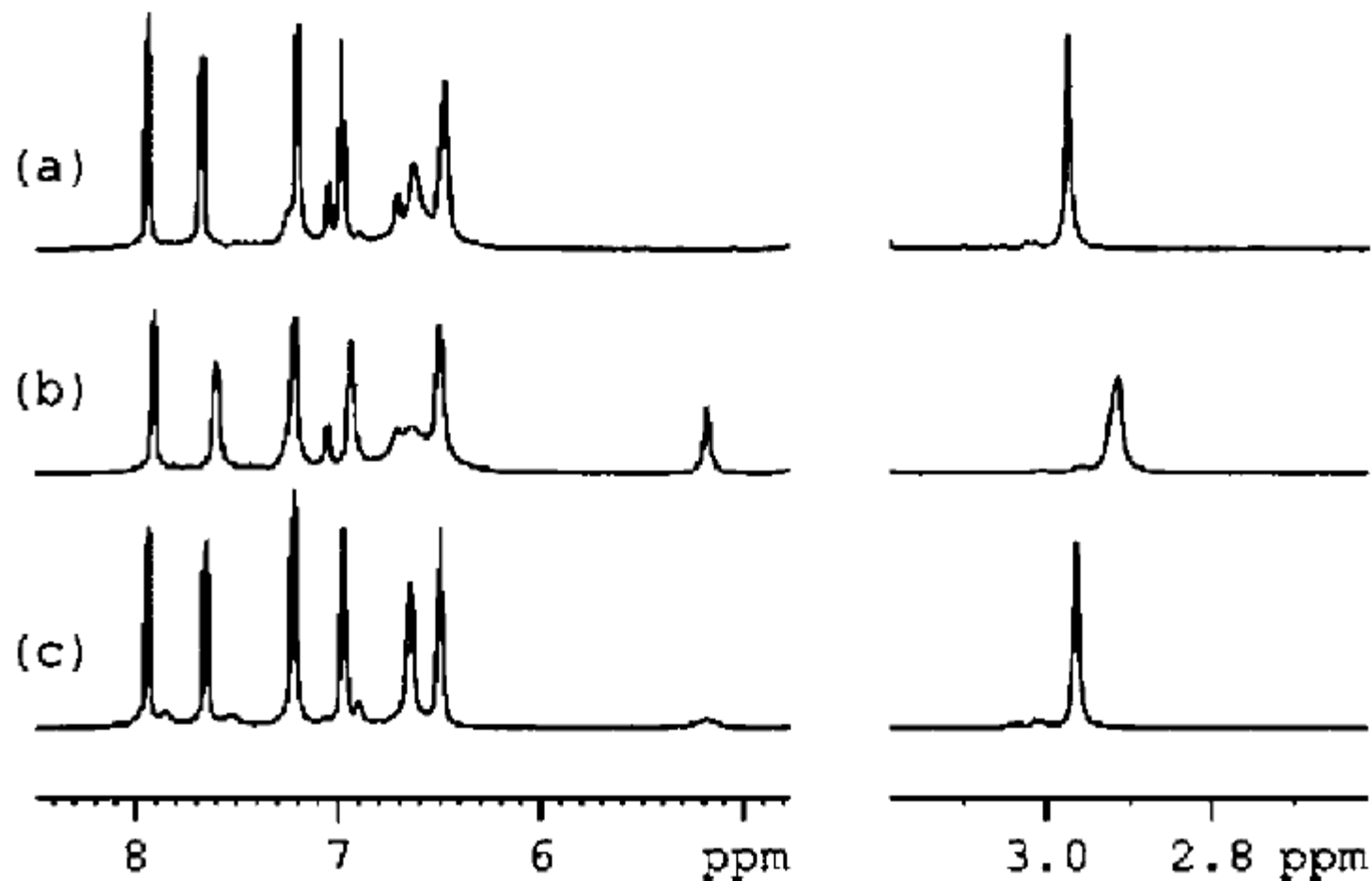
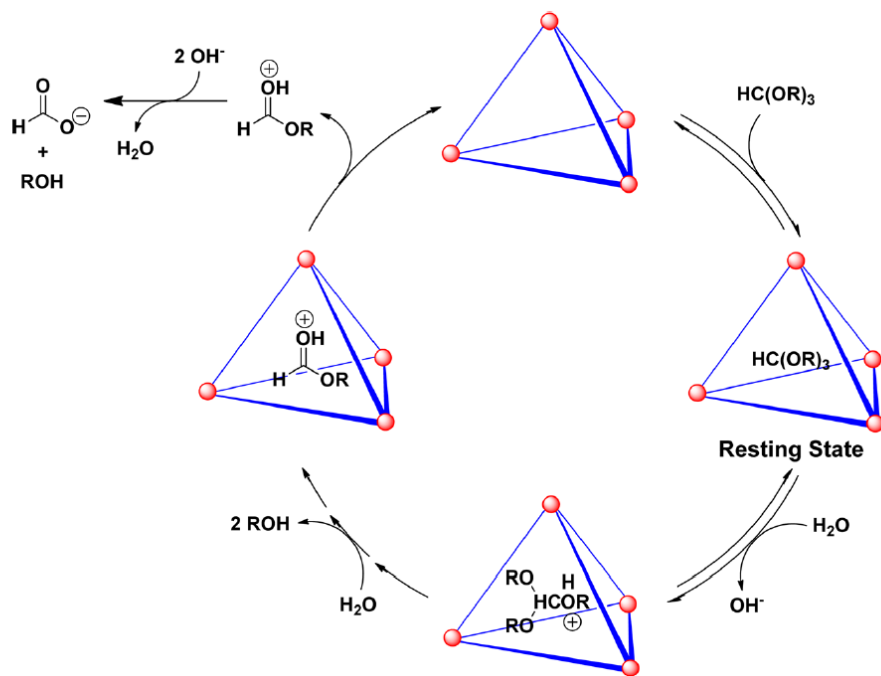


Figure 4. ^1H NMR spectra in D_2O of (a) the $[\text{Ga}_4\text{L}_6]^{12-}$ assembly + 1 equiv. **4**; (b) + 2 equiv. **4**; (c) sample in spectrum b after 20 h

Acid Catalysis in Basic Solution: A Supramolecular Host Promotes Orthoformate Hydrolysis

Michael D. Pluth, Robert G. Bergman,* Kenneth N. Raymond*



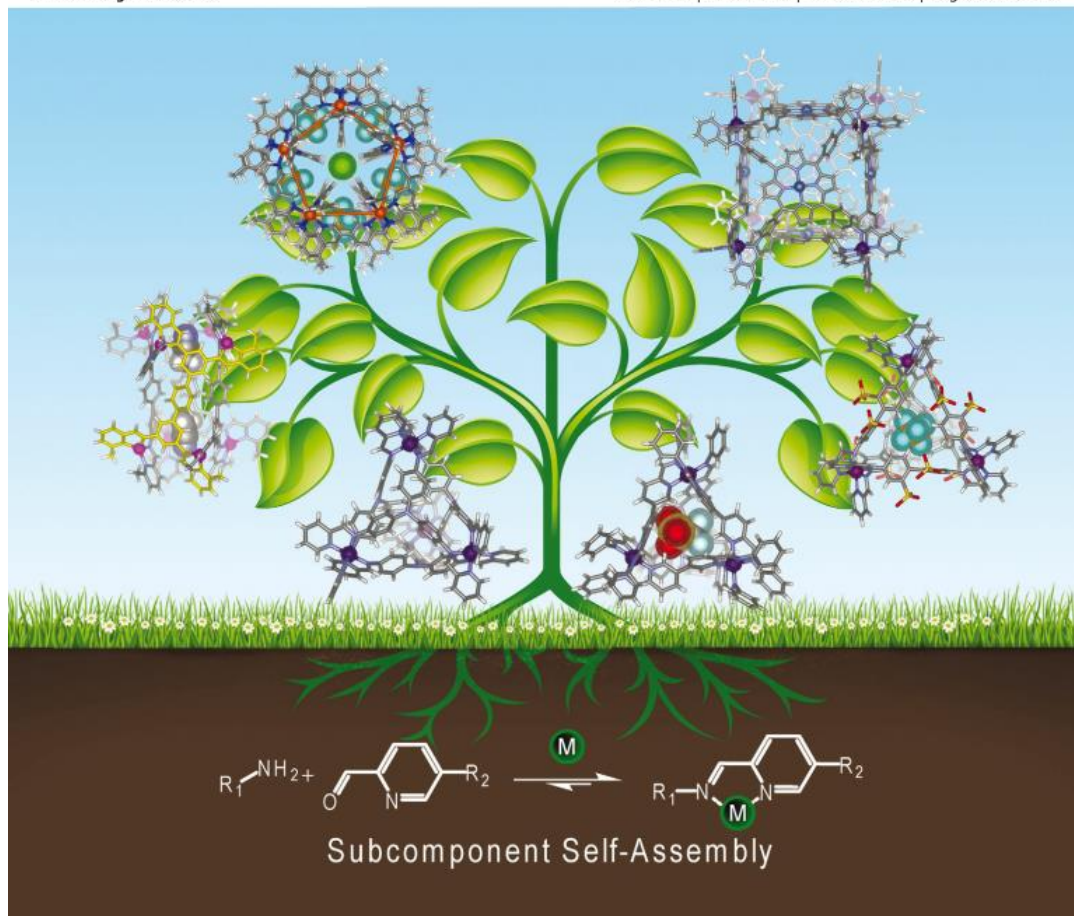
reached. Although the $\text{p}K_{\text{a}}$ of $\mathbf{3}\text{-H}^+$ is 10.8 in free solution, stabilization of the protonated form by **1**, which can be calculated as the product of the $\text{p}K_{\text{a}}$ and the binding constant of the protonated amine, shifts the effective basicity to 14.3 (32). This dramatic shift highlights the substantial stabilization of the protonated species over the neutral species upon encapsulation in the highly charged cavity (33).

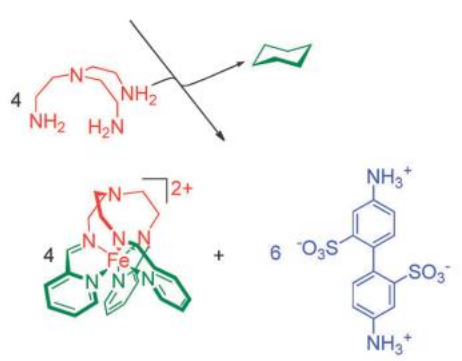
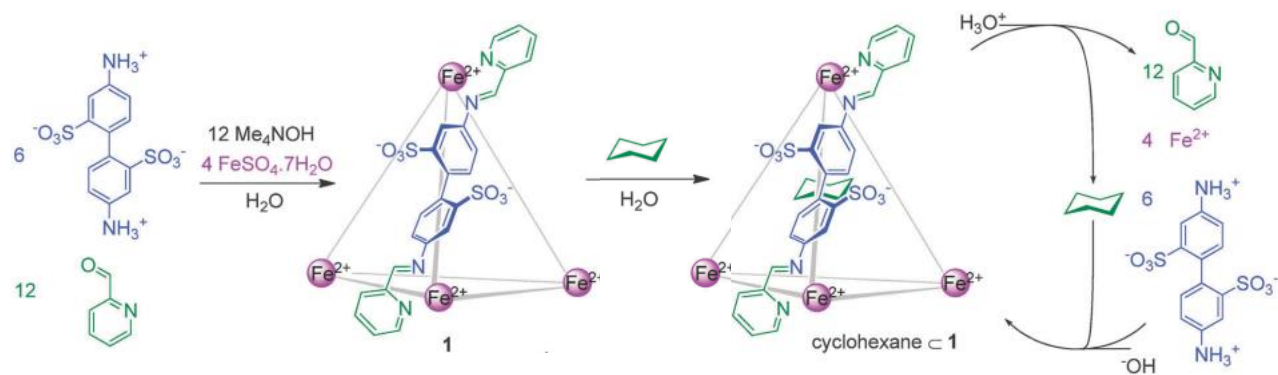
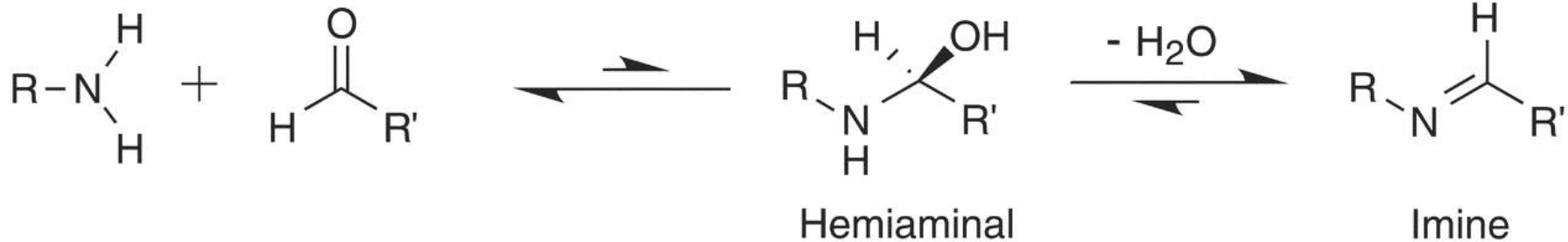
ChemComm

Chemical Communications

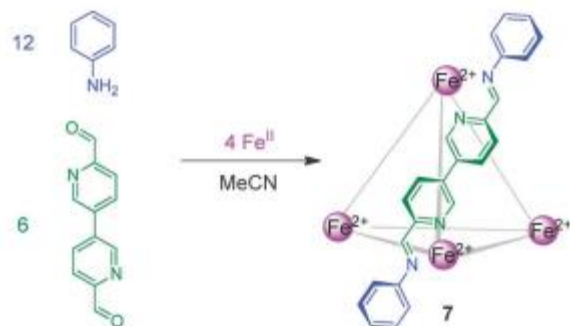
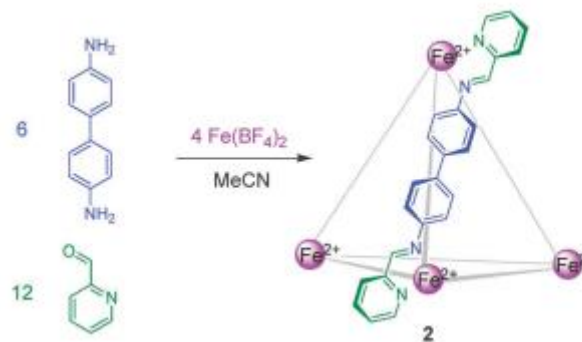
www.rsc.org/chemcomm

Volume 49 | Number 25 | 28 March 2013 | Pages 2465–2580

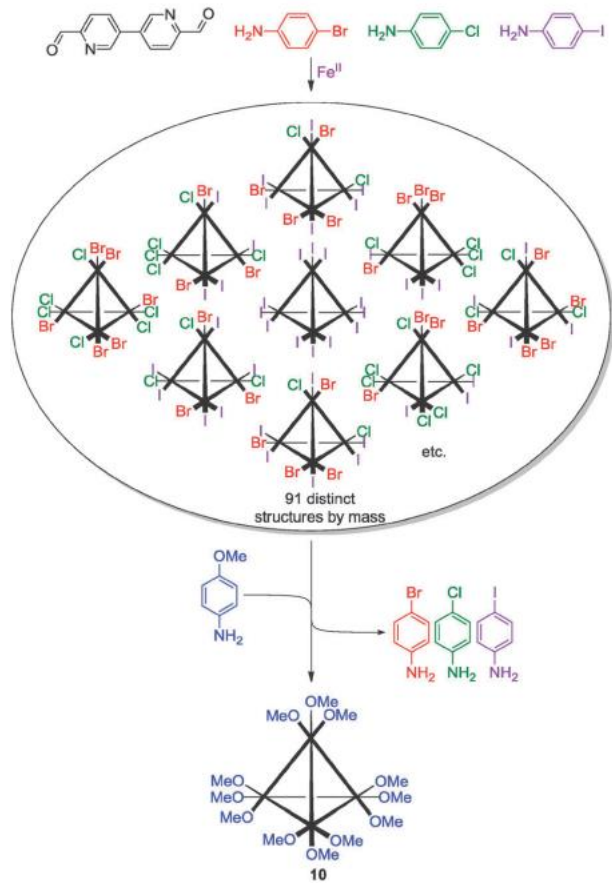
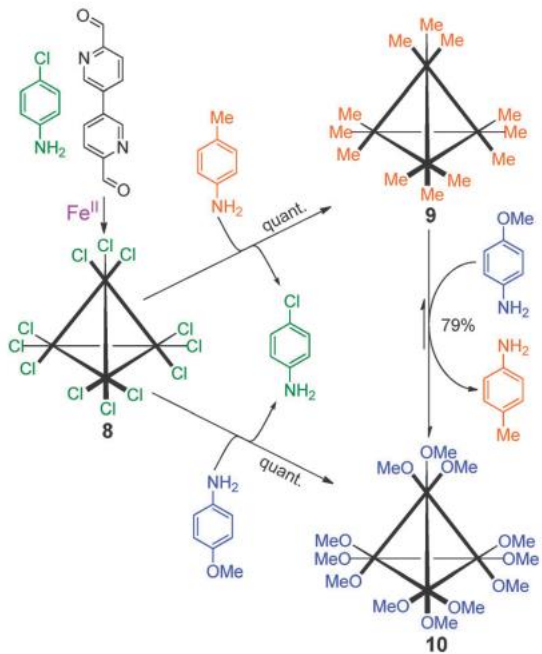


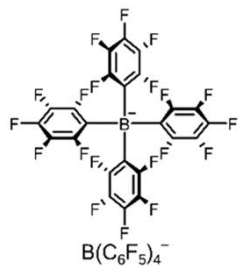
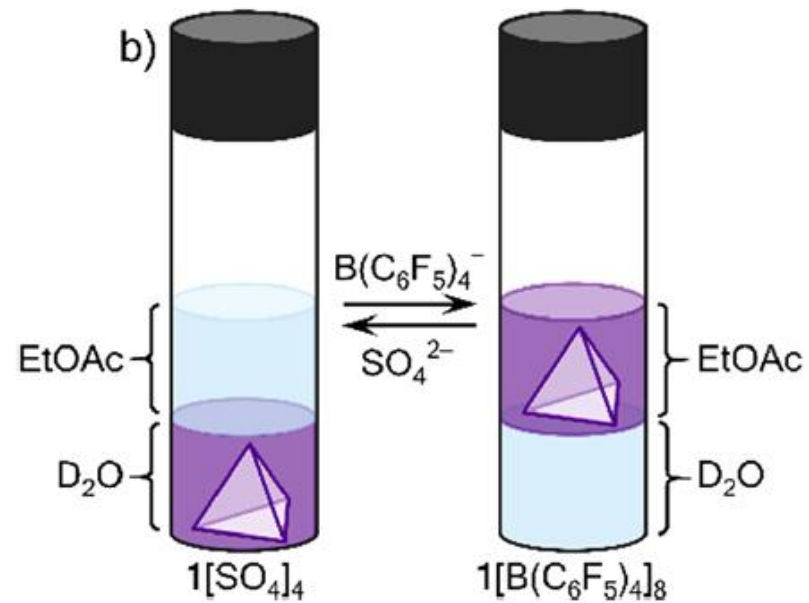
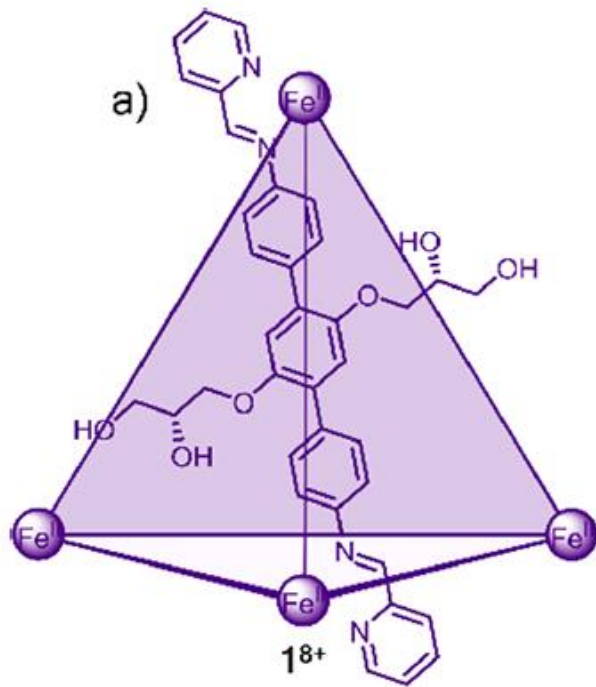


4,4'-diaminobiphenyl/2'-carboxyaldehyde



6,6'-diformyl-3,3'-bipyridine/aniline





LiB(C₆F₅)₄ to promote anion metathesis from SO₄²⁻ to B(C₆F₅)₄⁻

(*n*Bu₄N)₂SO₄ to regenerate the sulfate cage

White Phosphorus Is Air-Stable Within a Self-Assembled Tetrahedral Capsule

Prasenjit Mal,¹ Boris Breiner,¹ Kari Rissanen,² Jonathan R. Nitschke^{1*} SCIENCE VOL 324 26 JUNE 2009

1697

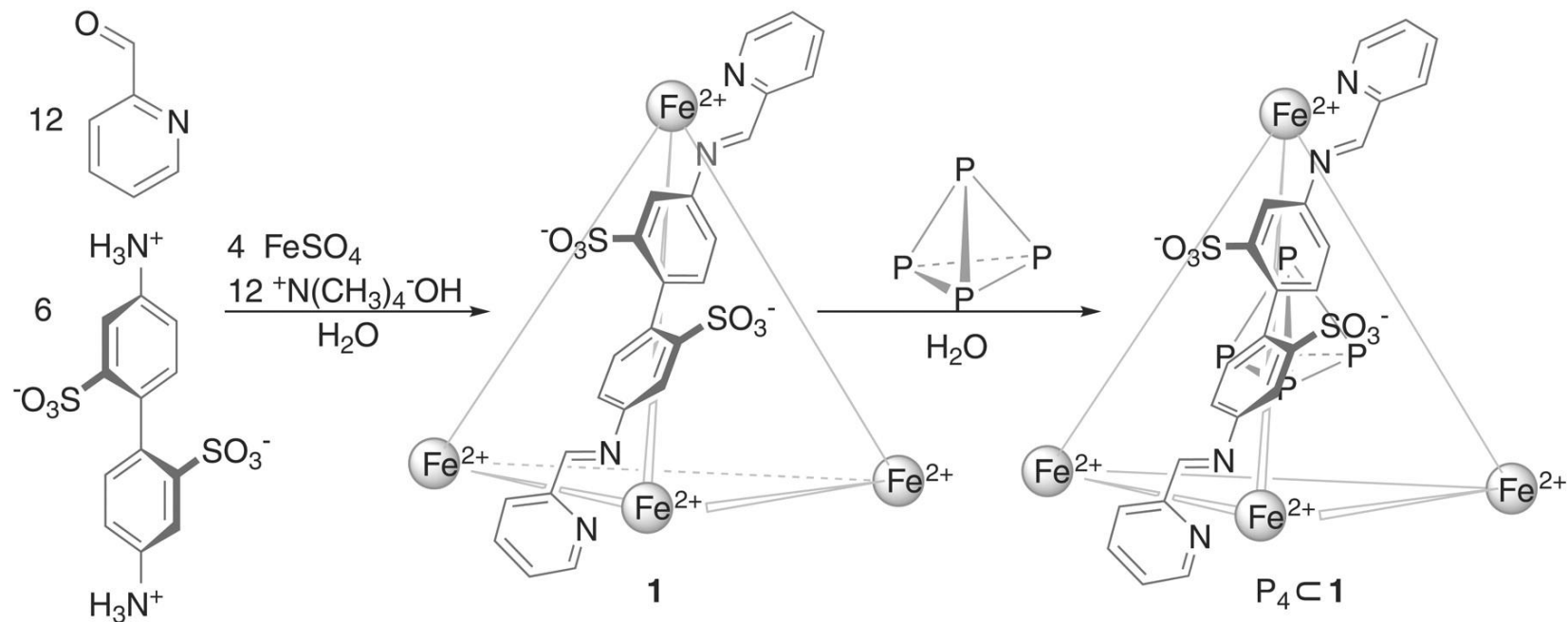


Fig. 1 Synthesis of tetrahedral cage 1 and subsequent incorporation of P₄.

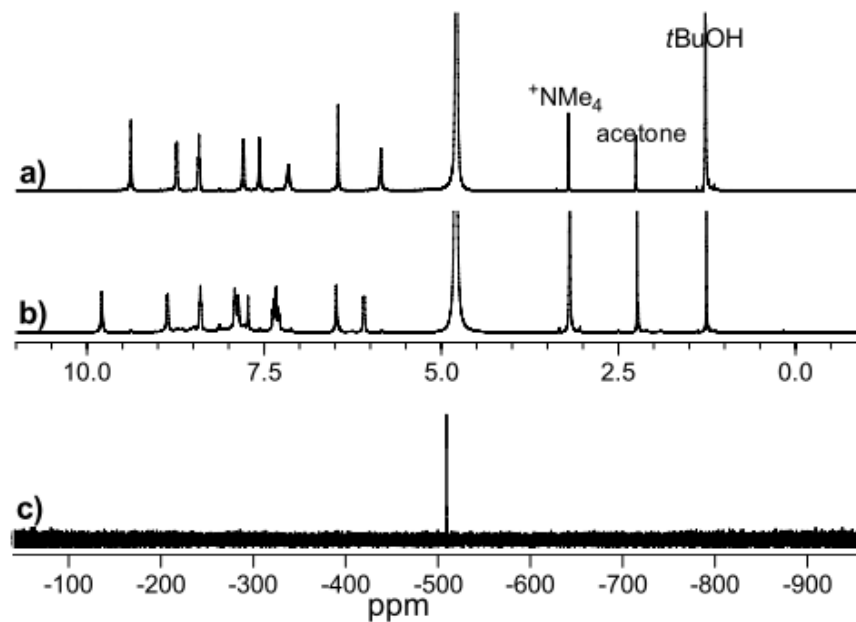


Figure S1. ^1H NMR spectra in D_2O of cage **1** (top), of $\text{P}_4\text{C1}$ (middle), and ^{31}P NMR spectrum of $\text{P}_4\text{C1}$ (bottom).

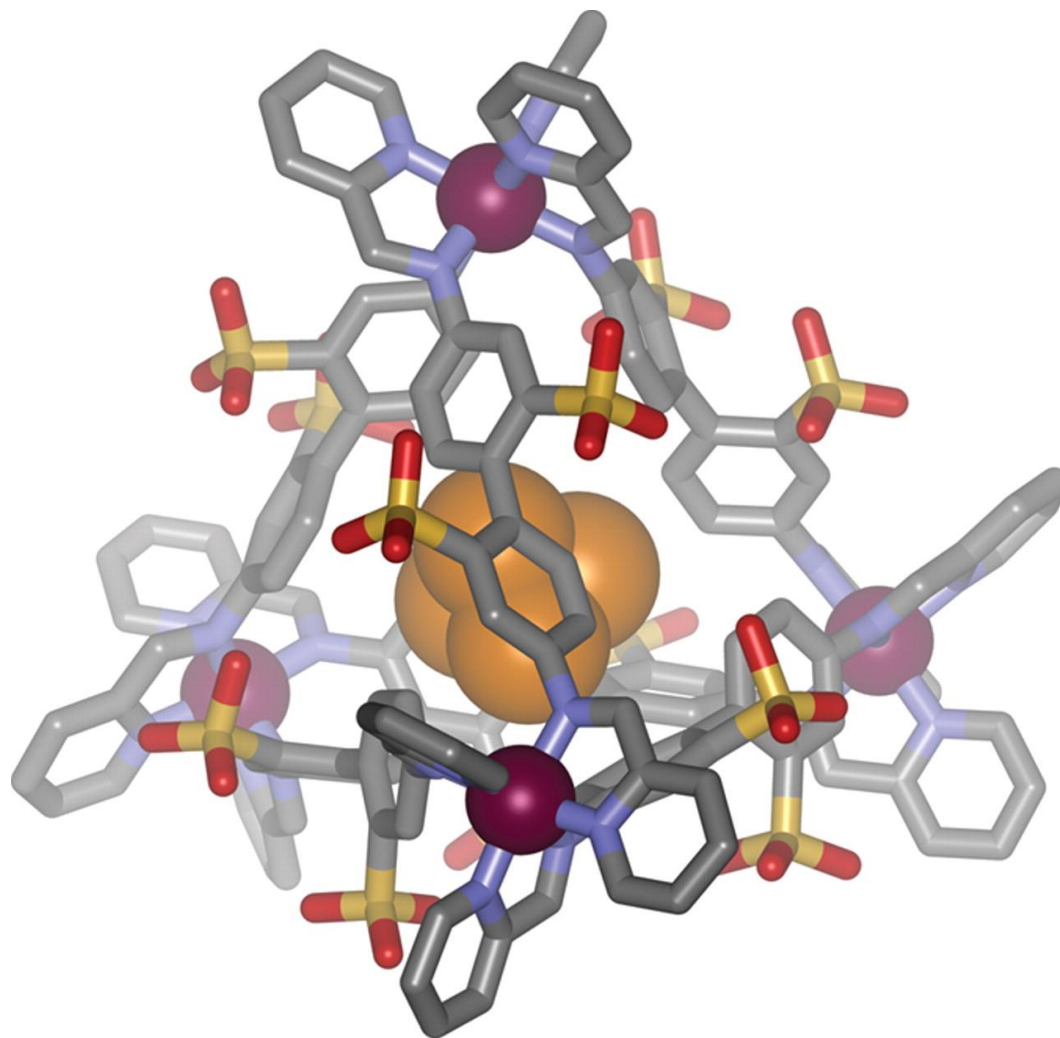


Fig. 2 Crystal structure of P4c1.

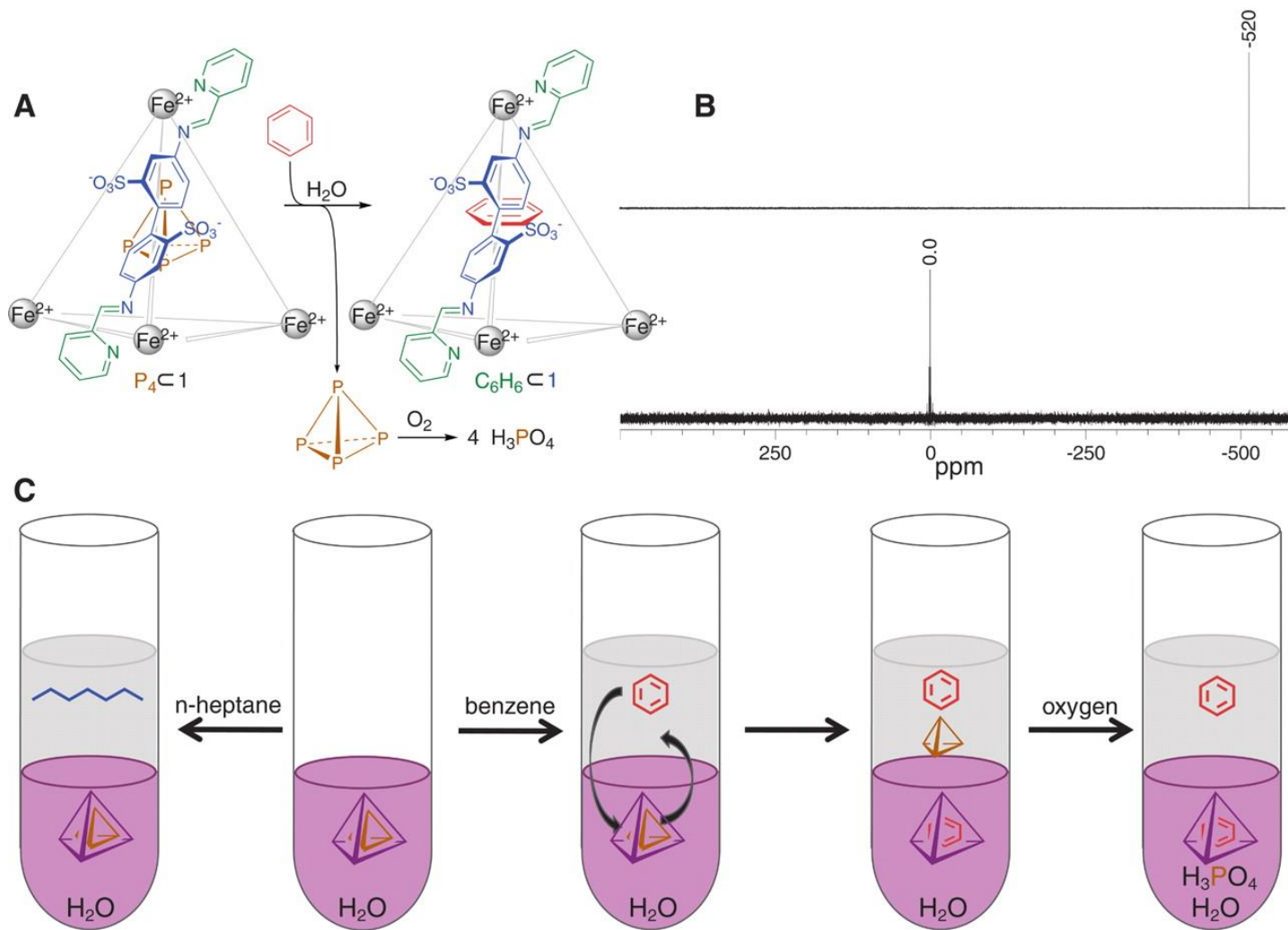
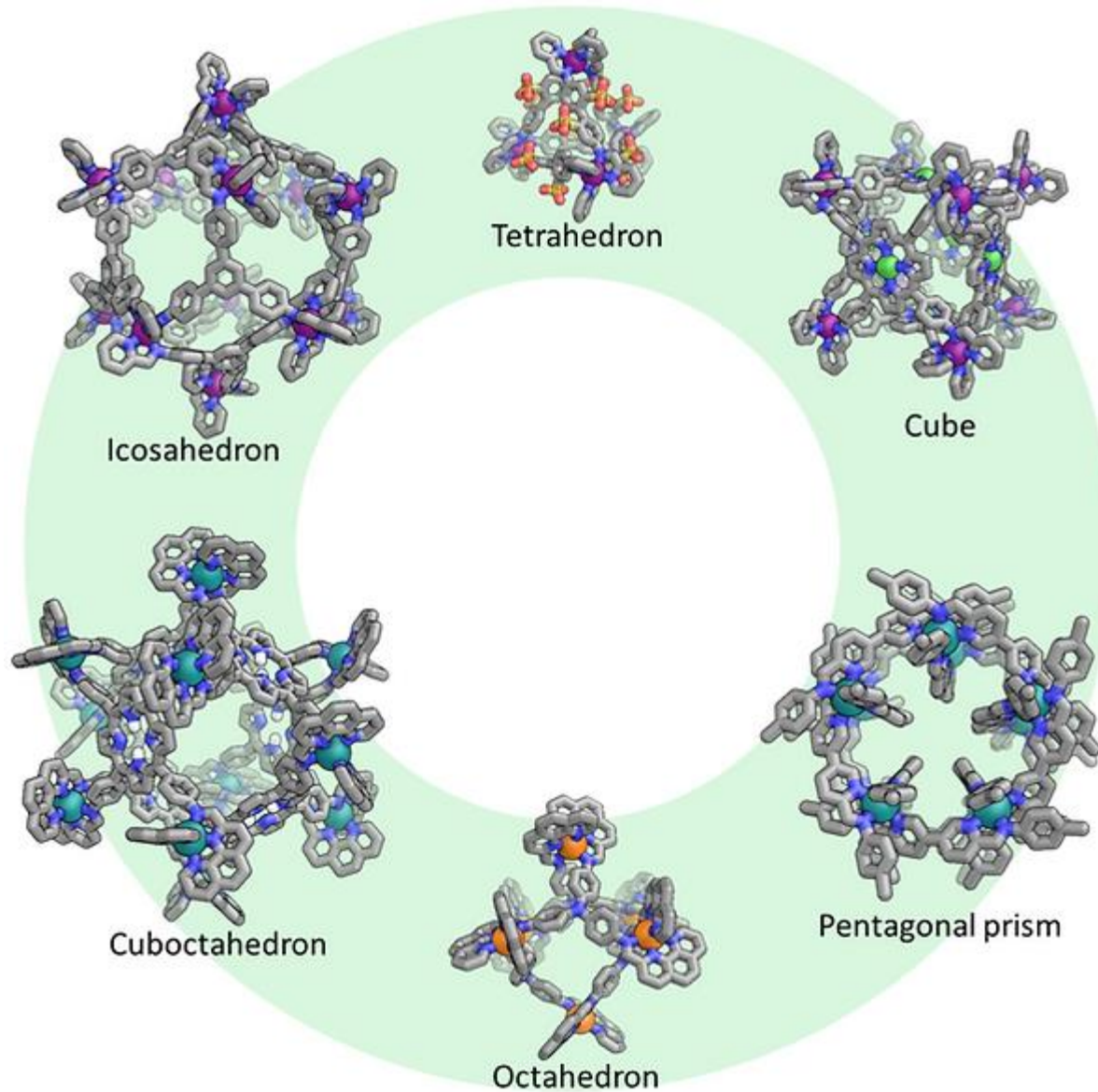


Fig. 3 Extraction of P4 from **1** by n-heptane is not possible, whereas replacing P4 with another suitable guest (benzene or cyclohexane) results in the facile removal of P4 into the organic solvent.

<https://www.nitschkegroup-cambridge.com/research-areas>



Design and Applications of Water-Soluble Coordination Cages

Edmundo G. Percástegui, Tanya K. Ronson, and Jonathan R. Nitschke*



Cite This: *Chem. Rev.* 2020, 120, 13480–13544



Read Online

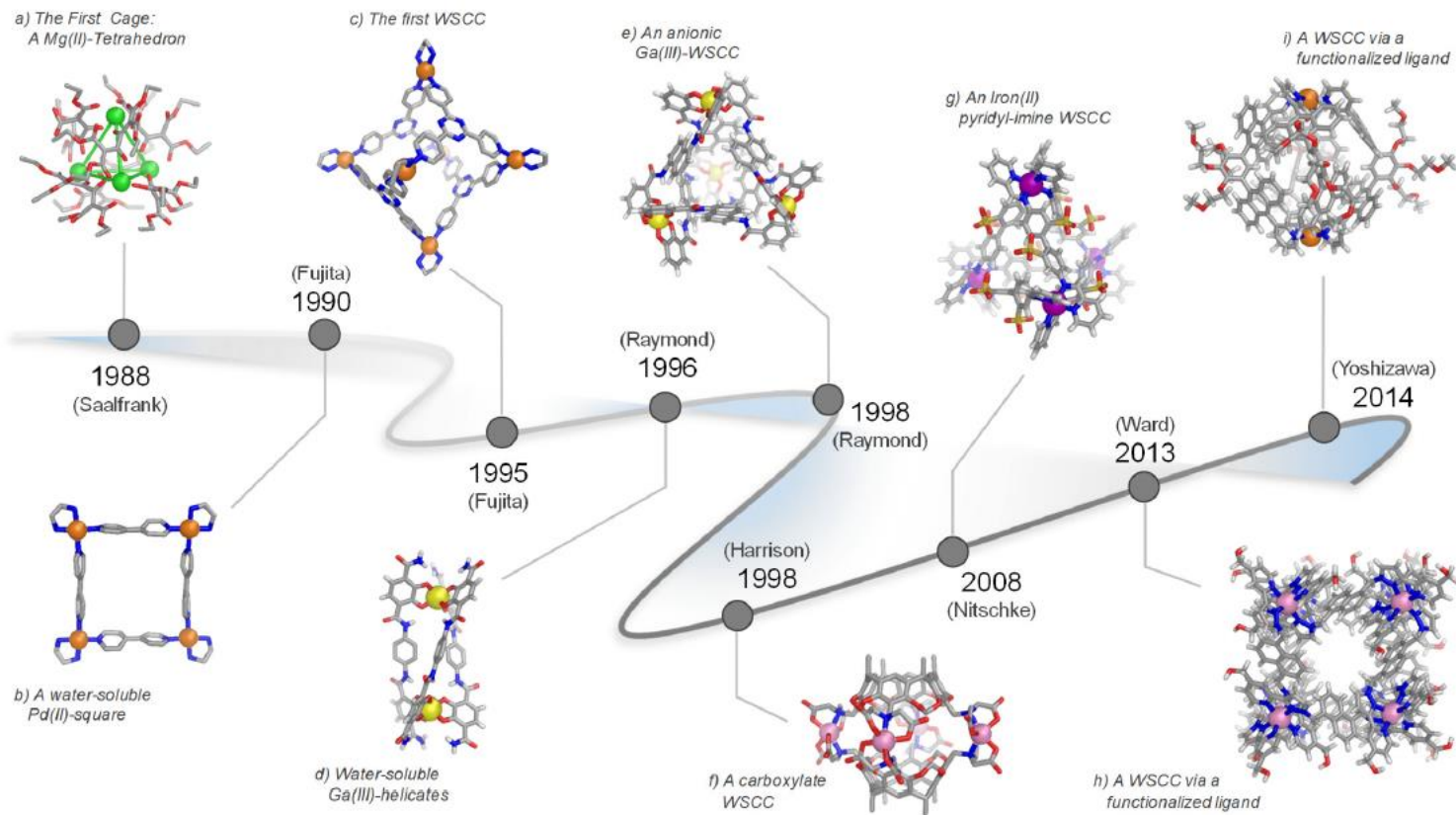


Figure 1. Timeline showing major advances in supramolecular coordination chemistry that have led from (a) the first cage complex to (b–f) early water-soluble complexes in the 1990s, and to (g–i) recent examples of WSCCs synthesized from ligands functionalized with solubilizing functional groups. The name of the group for each work is shown for reference.

Choice of metal ion - coordination geometry + kinetic lability:

Octahedral - Ga^{III}, Al^{III}, Ti^{IV}, Fe^{II}, Co^{II}, Zn^{II}, Cd^{II}, Ni^{II};

Square planar - Pd^{II} and Pt^{II}

Lanthanide ions kinetically labile BUT variable coordination number and geometry

Kinetically inert metal ions (e.g. Ru^{II} and Ir^{III}): kinetic control unless *trans* effect.

The self-assembly process - interplay between enthalpy and entropy:

multiple equilibria/variety of factors - metal coordination geometry/kinetic lability/ligand geometry/metal-to-ligand stoichiometry/concentration/solvent/presence of guests.

Therefore, it can be difficult to predict the outcome since there is a delicate.

The principle of maximum site occupancy:

species where all the metal coordination sites are occupied with ligands are more stable than those with vacant coordination sites since this maximises the number of metal–ligand bonds and therefore, the enthalpy.

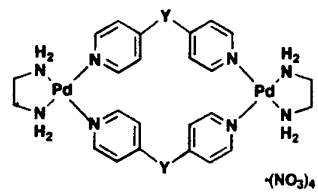
On the other hand, a system containing a larger number of smaller cages with fewer building blocks is favored on entropic grounds over one containing a smaller number of larger cages.

Multiple architectures can be self-assembled from the same building blocks:

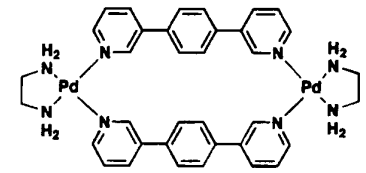
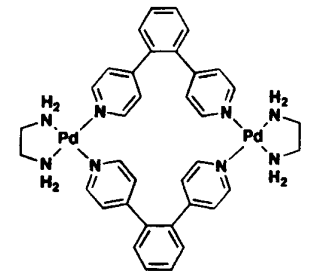
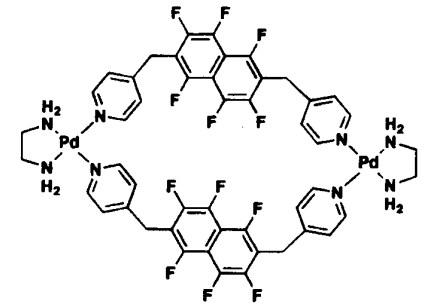
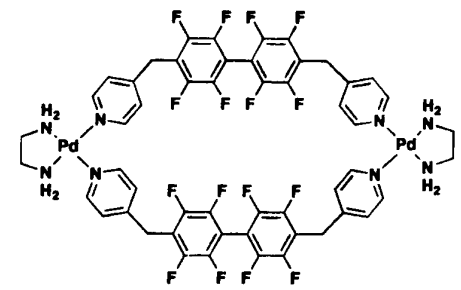
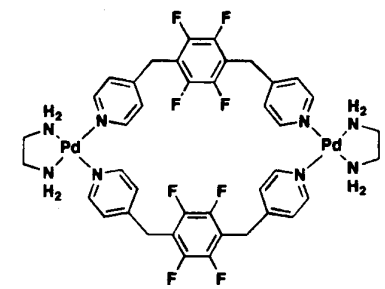
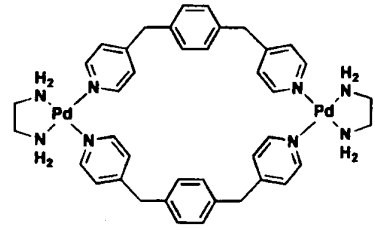
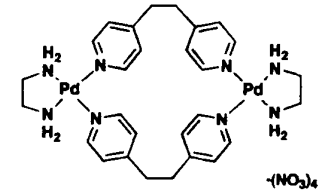
(a) a single cage when it is the thermodynamically most stable structure;

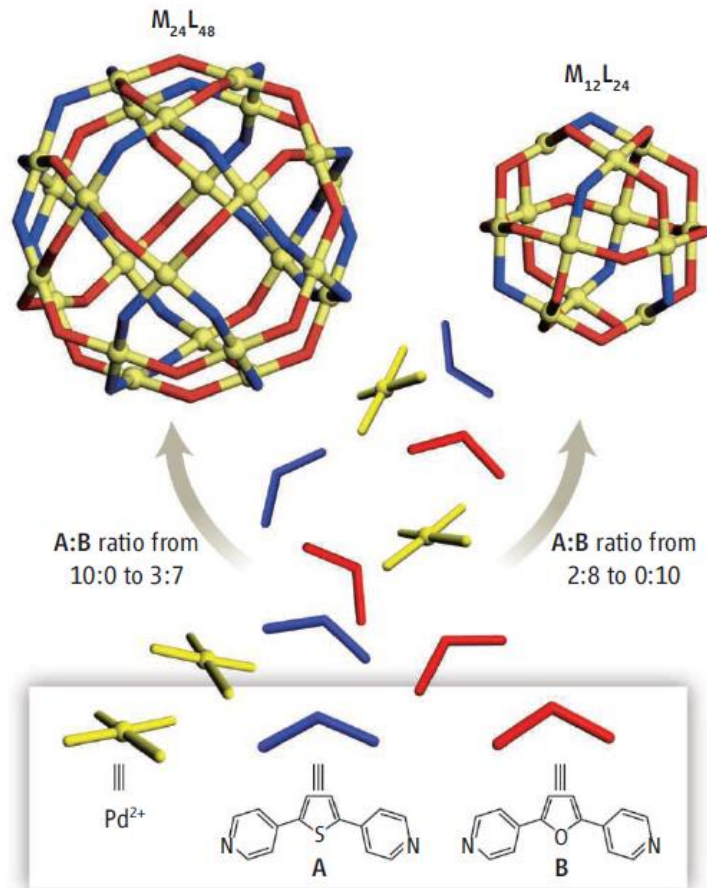
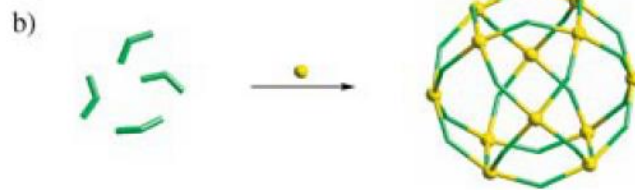
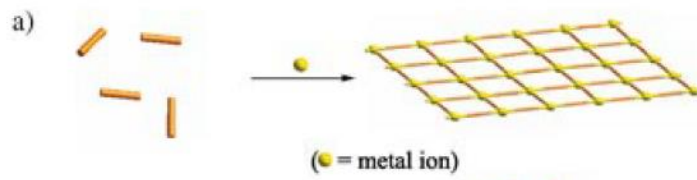
(b) a mixture of cages as the thermodynamic products with the distribution reflecting the relative energies of the cages;

(c) a dynamic combinatorial library with a large number of interconverting species in equilibrium.



Y = CH_2
 Y = $\text{C}(\text{OH})_2$





Design of lower symmetry cages

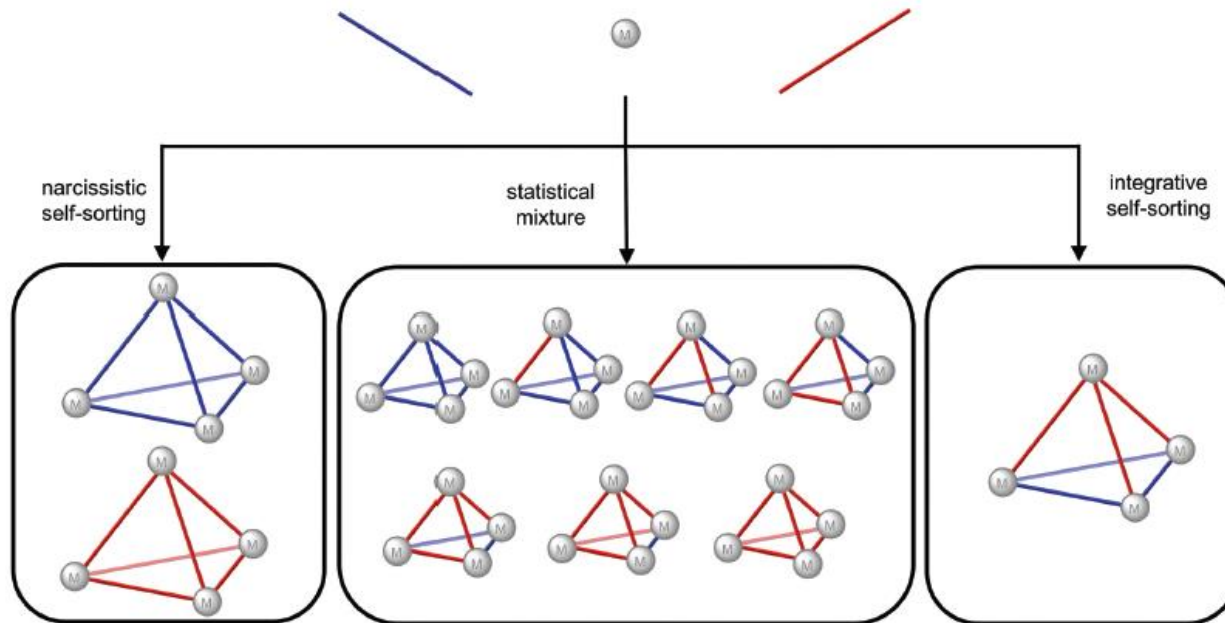
- symmetry breaking of the ligand upon metal coordination
- self-assembly of heteroleptic cages containing multiple ligands
- use of non-symmetric ligands to form homoleptic but lower symmetry cages
- use of multiple metals to form heterometallic cages.

Self-Sorting

narcissistic self-sorting - homoleptic cages with one ligand type in each cage

statistical mixture - both ligands are incorporated into the cages according to their statistical distribution;

integrative self-sorting - a nonstatistical distribution of heteroleptic cages results.



The key challenges to the design of heteroleptic cages via integrative self-assembly are, therefore, stabilisation of the heteroleptic cage/s relative to the homoleptic cages and biasing the system away from the statistical mixture.